Searches for rare top quark production and decay processes with the ATLAS experiment

Marcos Miralles López[1] on behalf of the ATLAS Collaboration

[1]IFIC (CSIC-UV) | marcos.miralles.lopez@cern.ch

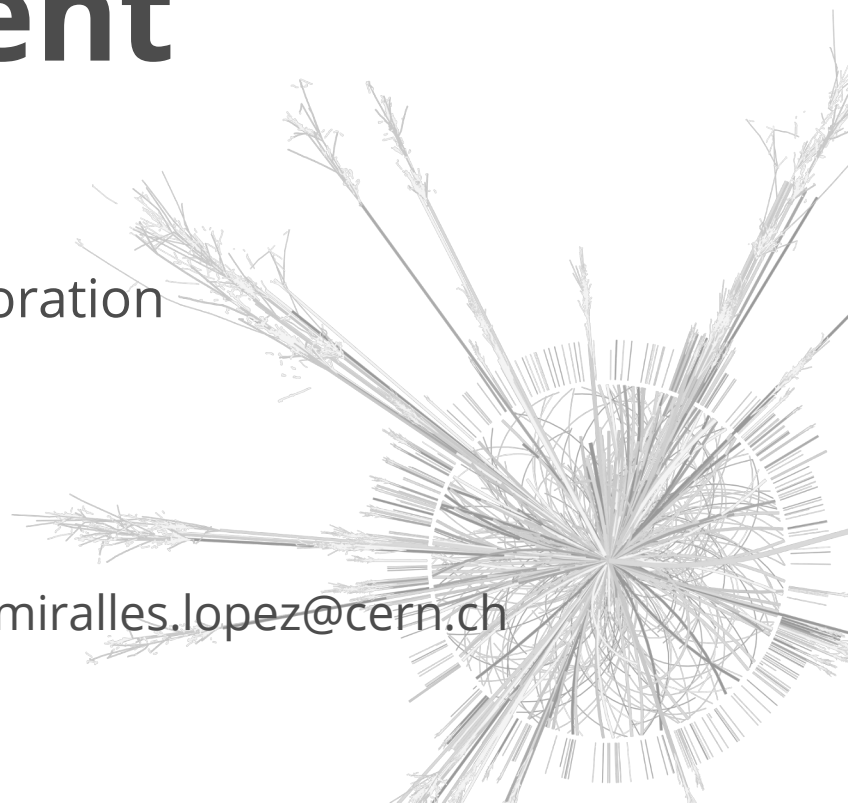

Overview

- Being the heaviest particle of the SM the **top-quark** is a good candidate for searching for **new physics**
  - **+ precision physics** (previous talk)
- The latest LHC data allow for **precise measurements of the top-EW sector**
- In this talk:
  - 4 tops measurement
  - Single top + photon observation
  - Flavour Changing Neutral Currents (FCNC) searches
    - $tq\gamma, tqZ, tqH, tqg$

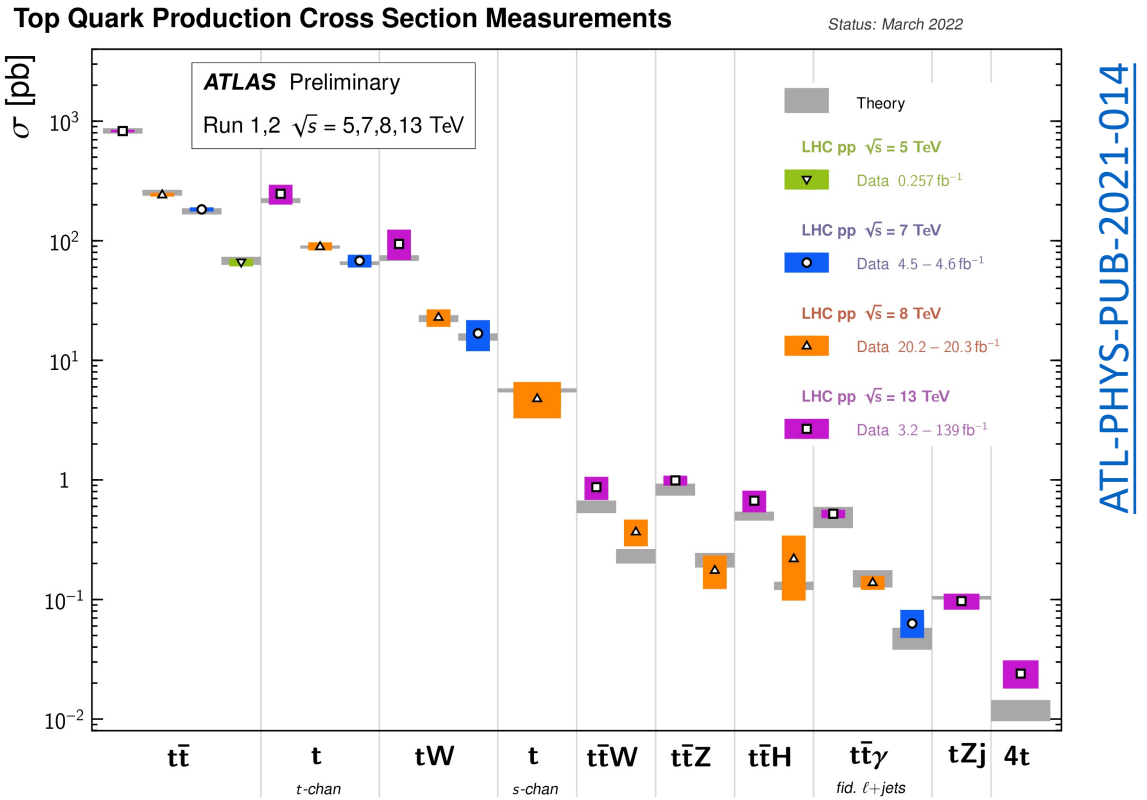

ATL-PHYS-PUB-2021-014

J. High Energ. Phys. **2021**, 118

Four-top-quark Analysis Strategy

- Most recent ATLAS 2LSS/3L @ 139 fb^{-1} with observed 4.3σ
  [Eur. Phys. J. C **80** (2020) 1085]
- Sensitive to top-Yukawa coupling and BSM interpretations
- **Event Selection**
  - Two categories: 1 lepton and 2 OS leptons
  - Categories splitted in jet and b-jet multiplicity
- **Background Estimation**
  - $t\bar{t}$+(HF) jets main background mismodelling is corrected
    - *Flavour Rescaling*: $t\bar{t}$ + light, $\geq 1c, \geq 1b$ yields are rescaled in four dedicated control regions in a profile-likelihood fit to data
    - *Sequential Kinematic Reweighing*: mitigates mismodelling of kinematic variables.
      - Events in the $\geq 3b$ regions are reweighed to data in $2b$ regions
  - Improved agreement and reduced systematics
- **Signal Extraction**
  - Separate BDTs are trained in SRs using 14 input kinematic variables to discriminate signal from background
  - **Maximum-likelihood fit** to all 21 SR+CR to extract $t\bar{t}t\bar{t}$ cross-section

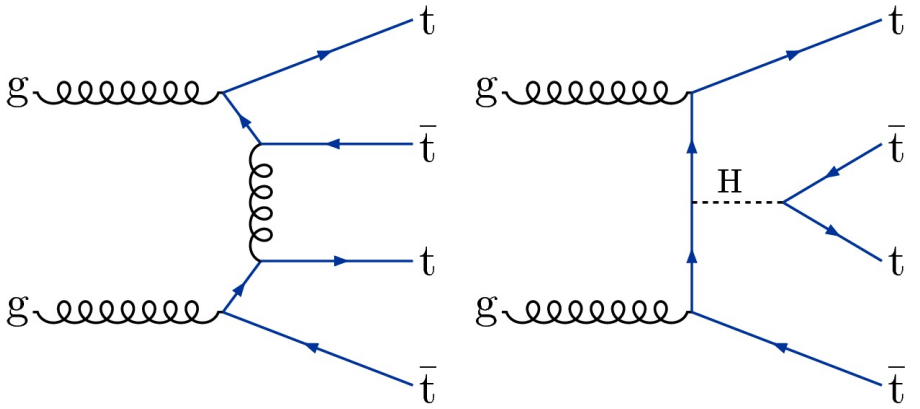

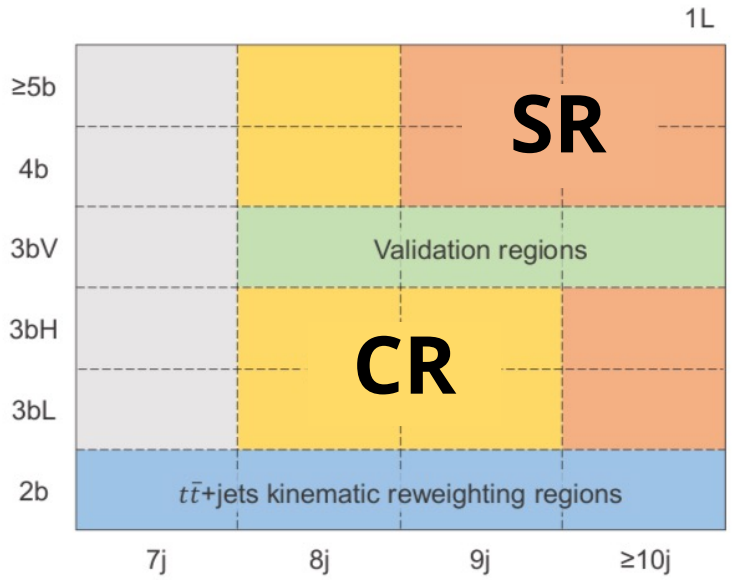

J. High Energ. Phys. **2021**, 118

Four-top-quark Results

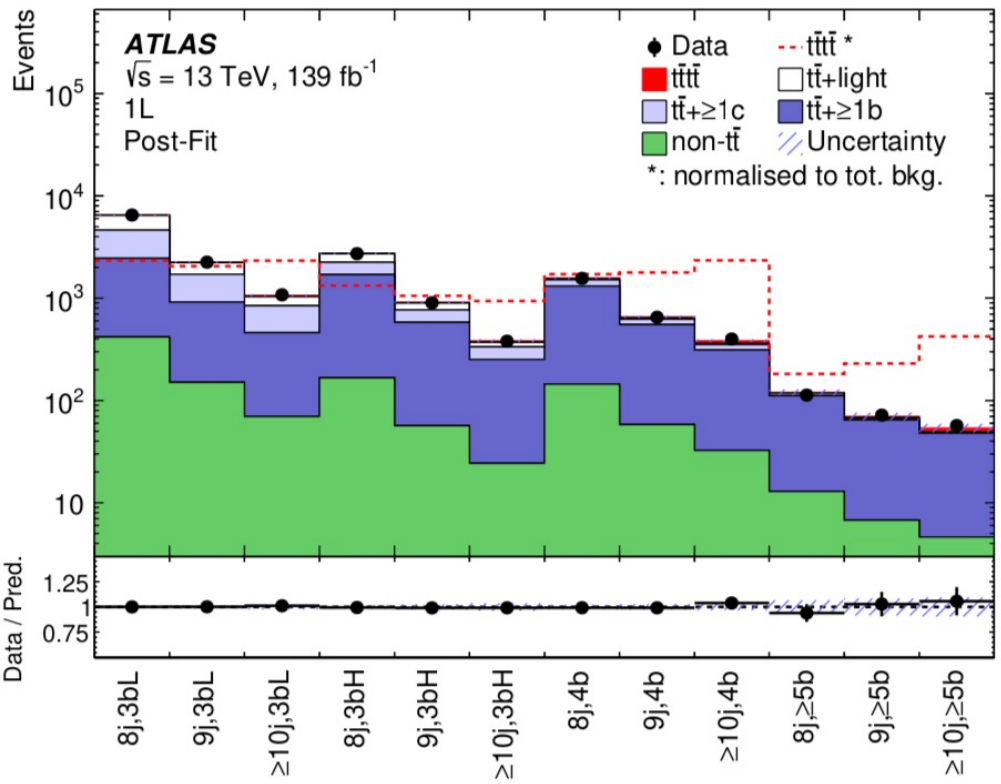

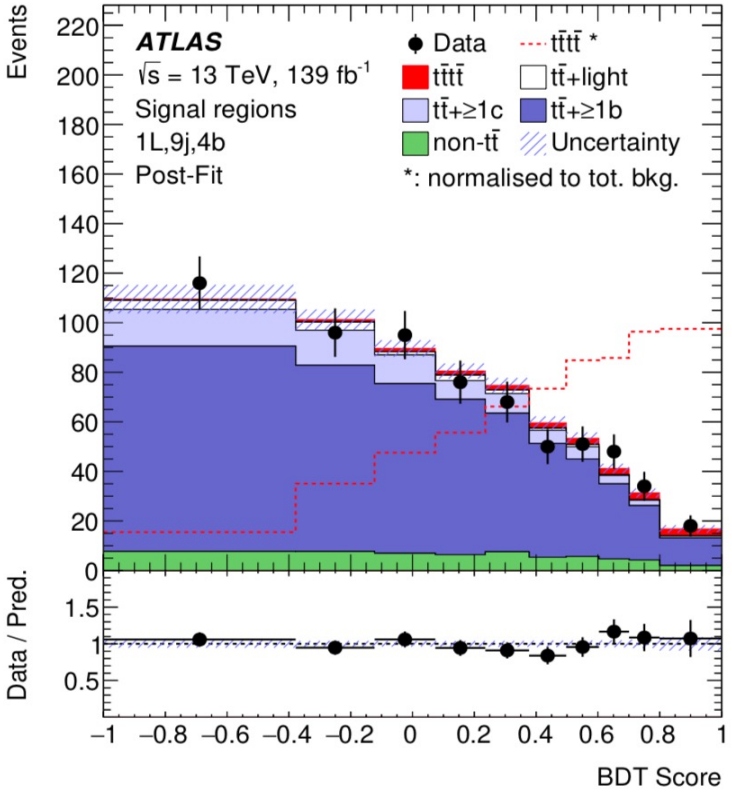

- Very comprehensive systematic model
  - Largest contribution from signal and $t\bar{t} + \geq 1b$ modelling
  - Systematic uncertainties dominate
- Excellent post-fit agreement

This result

- $\sigma_{t\bar{t}t\bar{t}} = 26 \pm 8(\text{stat.}) \,^{+15}_{-13}(\text{syst.}) = 26^{+17}_{-15}$ fb
- $\times 2.2$ SM prediction (within 1 std.)
- 1.9σ $(1.0)\sigma$ observed (expected) significance

Combination with ML results

- $\sigma_{t\bar{t}t\bar{t}} = 24 \pm 4(\text{stat.}) \,^{+5}_{-4}(\text{syst.}) = 24^{+7}_{-6}$ fb
- $\times 2.0$ SM prediction (within 2 stds.)
- **4.7σ $(2.6)\sigma$ observed (expected) significance**

Single top + photon Analysis Strategy

- Previous evidence from CMS @ 36fb^{-1} with 4.4σ [Phys. Rev. Lett. **121**, 221802]
- Probes $t + \gamma$ EW vertex [J. High Energ. Phys. **2022,** 32]
- **Event Selection**
  - $= 1$ central lepton, $= 1$ central photon, $= 1$ b-tagged jet* (70% WP), $E_{\mathrm{T}}^{\mathrm{miss}} > 30$ GeV, $|m_{e\gamma} - 90| > 10$ GeV
  - **Two SRs:** $= 0$ fwd jets, ≥ 1 fwd jet ($2.5 < |\eta| < 4.5$)
- **Background Estimation**
  - $t\bar{t}\gamma$ and $W\gamma$ main backgrounds are estimated in dedicated control regions
    - $t\bar{t}\gamma$ uses a NN distribution while $W\gamma$ only has one bin
  - $e \to \gamma$ ($t\bar{t}$ dilepton) and $h \to \gamma$ ($t\bar{t}$ l+jets) fakes using data-driven methods
- **Signal Extraction**
  - 2 NNs are used to enhance the signal for each signal region
    - Using 12/15 input variables based on final-state kinematics and b-tag properties
    - Shapes of inputs are well modelled by data
  - **Maximum-likelihood fit** to all 4 SR+CR with 3 free-floating parameters: signal, $t\bar{t}\gamma$ and $W\gamma$

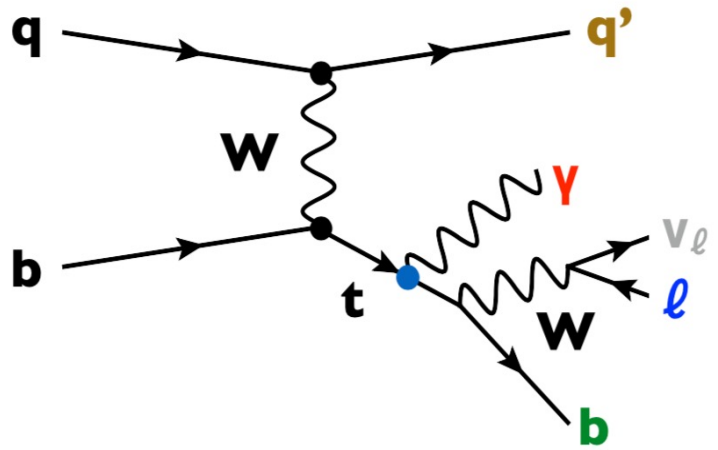

*Events with 2nd b-jet (85% WP) are vetoed

Single top + photon Results

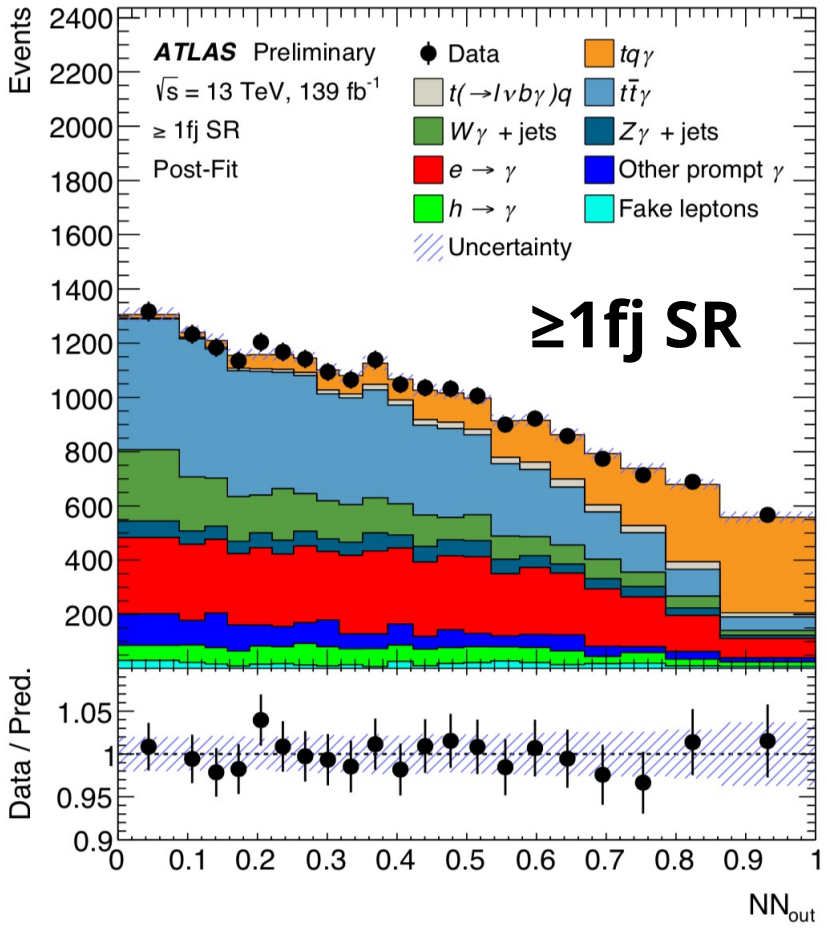

- **Main systematic uncertainties**
  - $t\bar{t}$ and $t\bar{t}\gamma$ modelling
  - Background limited MC statistics
  - Jet and $E_{\mathrm{T}}^{\mathrm{miss}}$
  - Fake contributions are smaller in comparison
- **The observed (expected) significance is 9.1σ (6.7)σ**
- **Parton-Level** Fiducial cross-section
  - $\sigma_{tq\gamma} \times \mathcal{B}(t \to lvb) = 580 \pm 19(\mathrm{stat.}) \pm 63(\mathrm{syst.})$ fb
- **Particle-Level** Fiducial cross-section
  - $\sigma_{tq\gamma} \times \mathcal{B}(t \to lvb) + \sigma_{(t \to lvb\gamma)q} = 287 \pm 8(\mathrm{stat.}) \pm 31(\mathrm{syst.})$ fb
- Measurements are within **2.5σ** and **1.9σ** of the SM predictions for Parton and Particle-level respectively
  - With the measurement being higher than the prediction for both

Flavour Changing Neutral Currents

- FCNC are **forbidden** at Born level and **highly supressed** at loop level in the SM due to GIM mechanism
- Any observation of enhanced rates would be clear evidence of BSM
- Several BSM models also set bounds on the FCNCs BRs
  - 2HDM, RPV SUSY, MSSM, RS, … [arXiv: 1311.2028]
- FCNC vertex in **production** and **decay** modes is treated in a model independent way in an **EFT** framework
  - Limits from cross-sections reinterpreted as limits on EFT Wilson coefs. and BRs
- Results are separated for $u(c)$ valence (sea) quarks to due the different PDFs

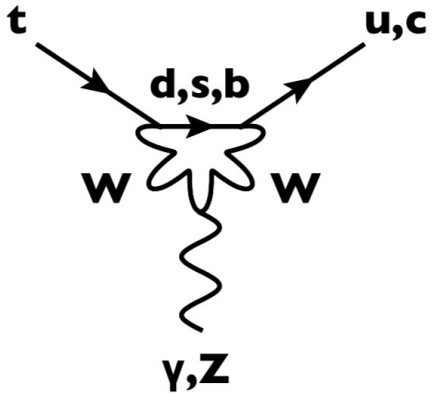

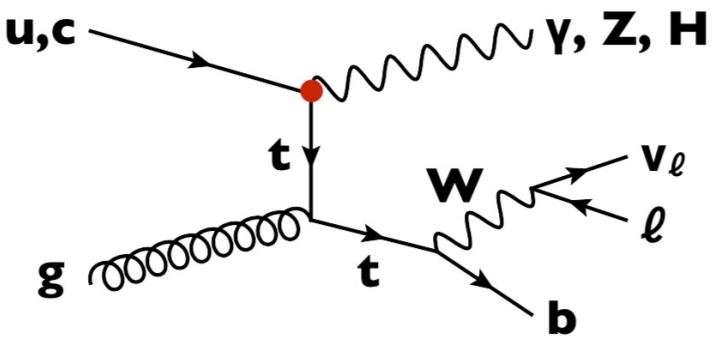

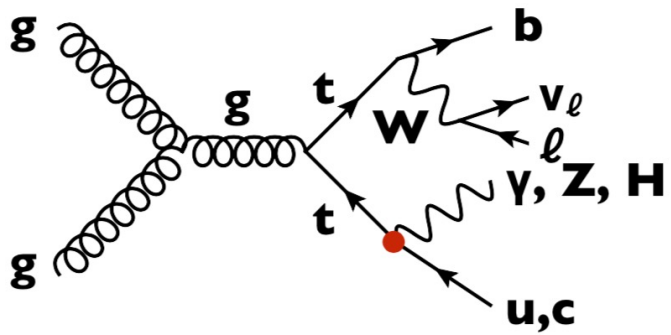

arXiv:hep-ph/0409342	SM $\mathcal{BR}$(u)	SM $\mathcal{BR}$(c)
$t \to \gamma + u/c$	4×10^{-16}	5×10^{-14}
$t \to Z + u/c$	8×10^{-17}	1×10^{-14}
$t \to H + u/c$	2×10^{-17}	3×10^{-15}
$t \to g + u/c$	4×10^{-14}	5×10^{-12}

FCNC $tq\gamma$ Analysis Strategy

ATLAS-CONF-2022-003

- Analysis is optimised in both FCNC production and decay mode
- Shares many similarities with SM $tq\gamma$ analysis
  - Same final-state, main background ($t\bar{t}\gamma$ and $W\gamma$) and fake ($e \to \gamma$ and $h \to \gamma$) estimation techniques
  - No separation of SRs in forward jets
- **Signal Extraction**
  - Multi-class NN are trained for each region and up or charm quarks
    - 37 input variables from final-state kinematics and photon conversions
    - 3 output nodes: $y_{\text{prod}}, y_{\text{decay}}, y_{\text{bkg}}$
    - This approach is ~30% better than optimised binary classifier
  - **Maximum-likelihood fit** to all 3 SR+CR to obtain limits on EFT WC and BRs

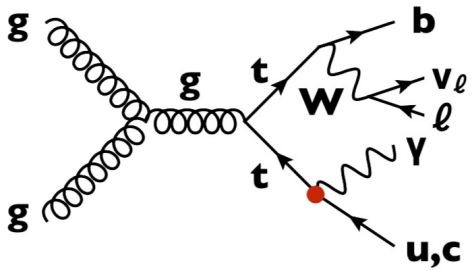

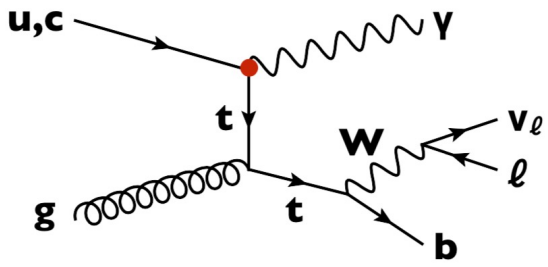

SR bkg. composition

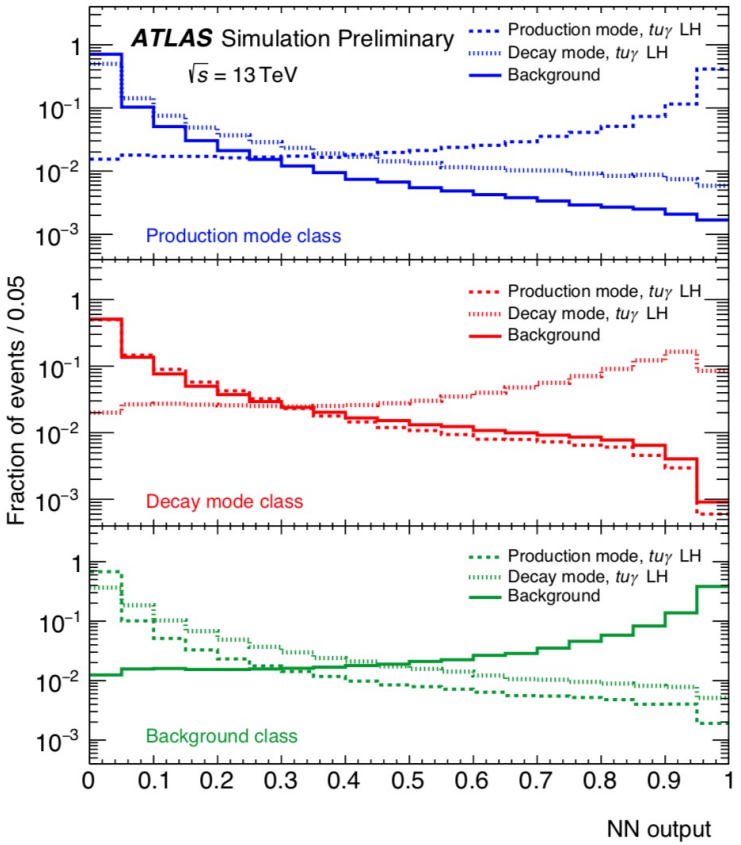

FCNC $tq\gamma$ Results

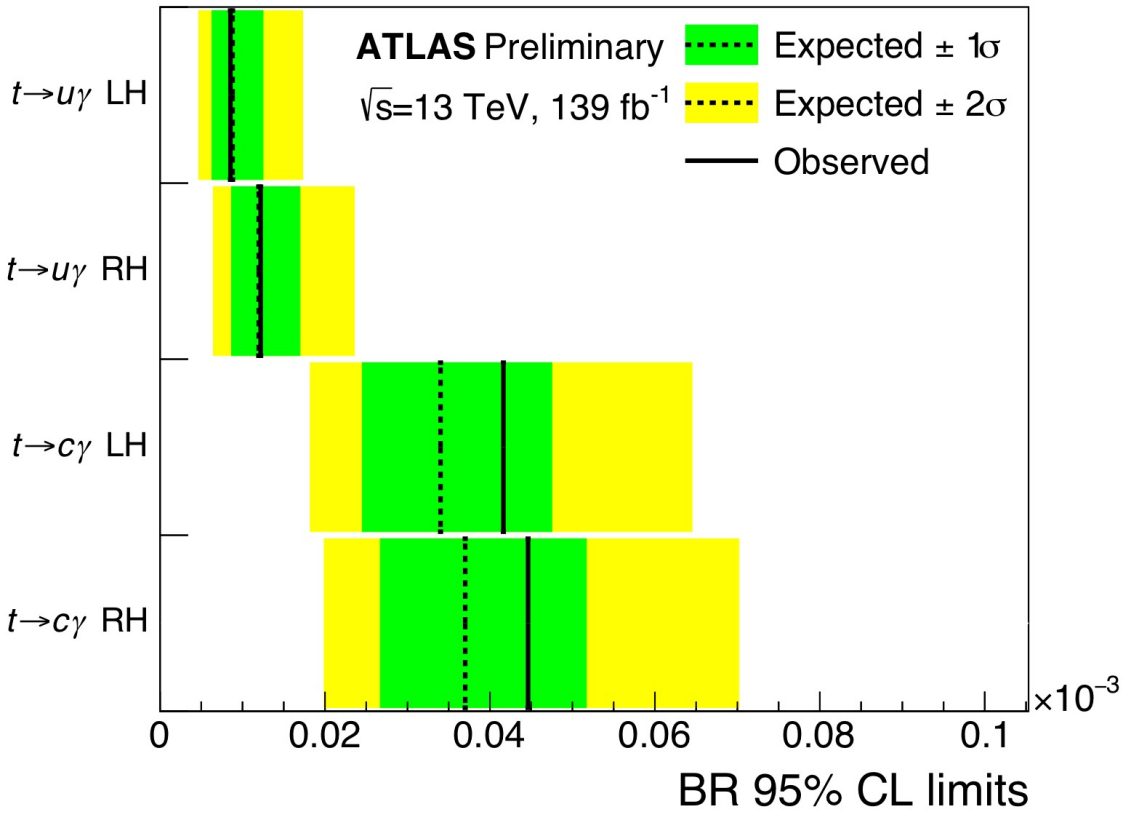

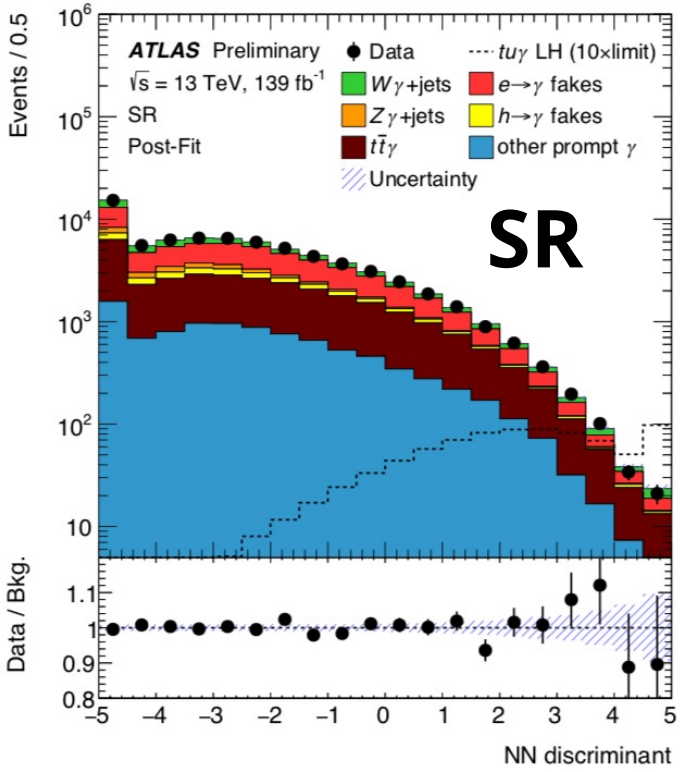

Stat. and syst. uncertainties

- Analysis is dominated by statistical uncertainties
- Leading syst. unc.: $tq\gamma$ SM cross-section

- Previous ATLAS 81fb^{-1} (focus on production mode) [Phys. Lett. B 800, 135082]
- These results present a **factor 3.3–5.2 improvement** with respect to the previous search
- Adding events with additional jets (decay mode), optimised signal region and analysis strategy, more luminosity (139 fb^{-1})

FCNC tqZ Analysis Strategy

- Analysis is optimised in both FCNC production and decay modes
- **Event Selection**
  - $Z \to ll$, semi-leptonic top decay: $= 3$ isolated leptons $p_{\mathrm{T}} > 27/15/15$ GeV, $= 1$ b-tagged jet (70% WP)
  - **Two SRs:** targeting decay SR1 (≥ 2 jets), targeting production SR2 (≥ 1 jet, $m_{l\nu} > 40$ GeV)
- **Background Estimation**
  - $t\bar{t}$ and $t\bar{t}Z$ main backgrounds are estimated in dedicated control regions
  - VV+HF are estimated in 2 sideband control regions
- **Signal Extraction**
  - χ^2 minimisation technique is used to reconstruct kinematics of top quark candidates
  - Three separate BDTs are trained to discriminate signal from background
    - SR1 (D_1): both FCNC tuZ and tcZ decay modes
    - SR2 (D_2^u): FCNC tuZ production mode
    - SR2 (D_2^c): FCNC tcZ for both production and decay modes
  - **Maximum-likelihood fit** to all 6 SR+CR to obtain limits on EFT WC and BRs

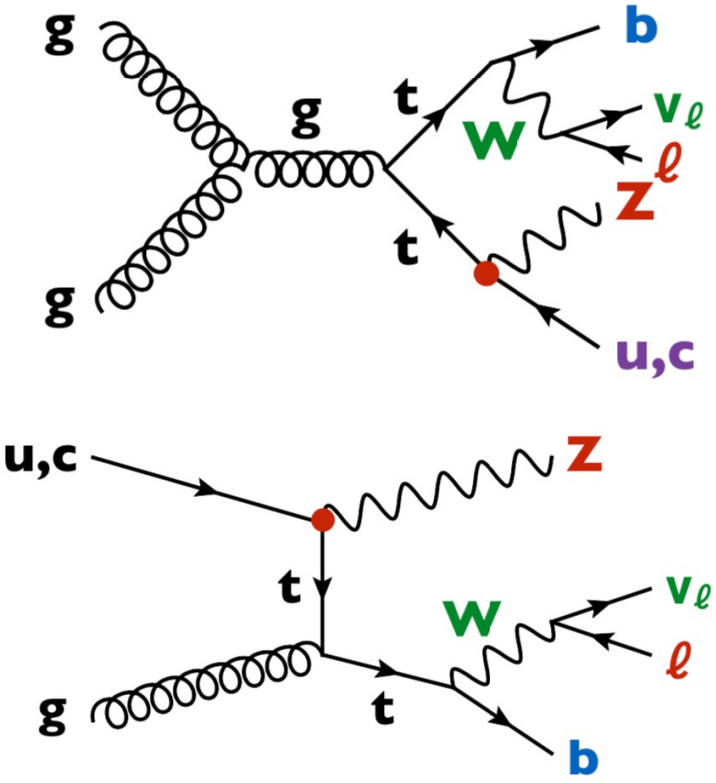

FCNC tqZ Results

ATLAS-CONF-2021-049

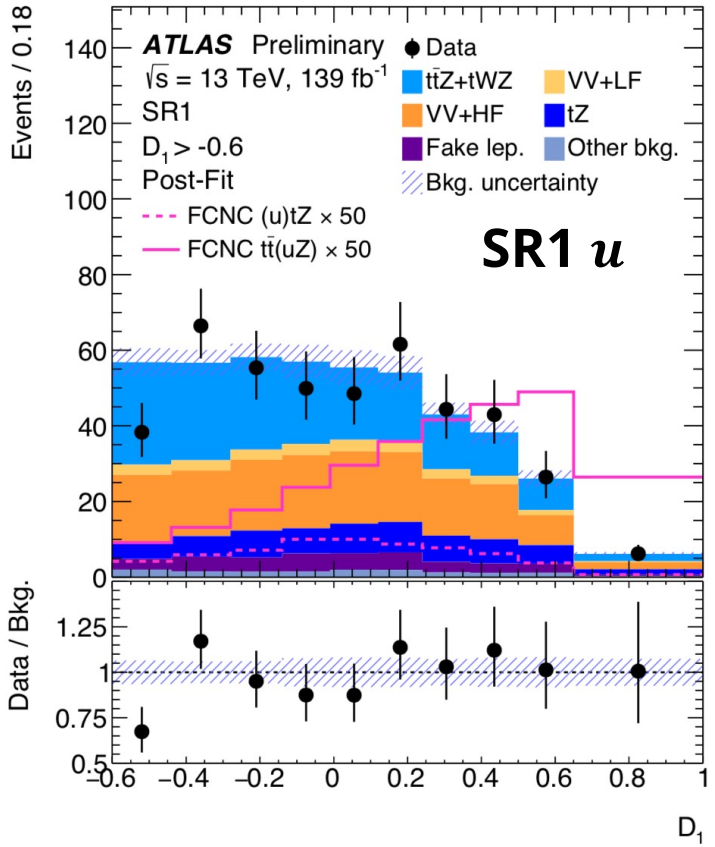

Decay mode

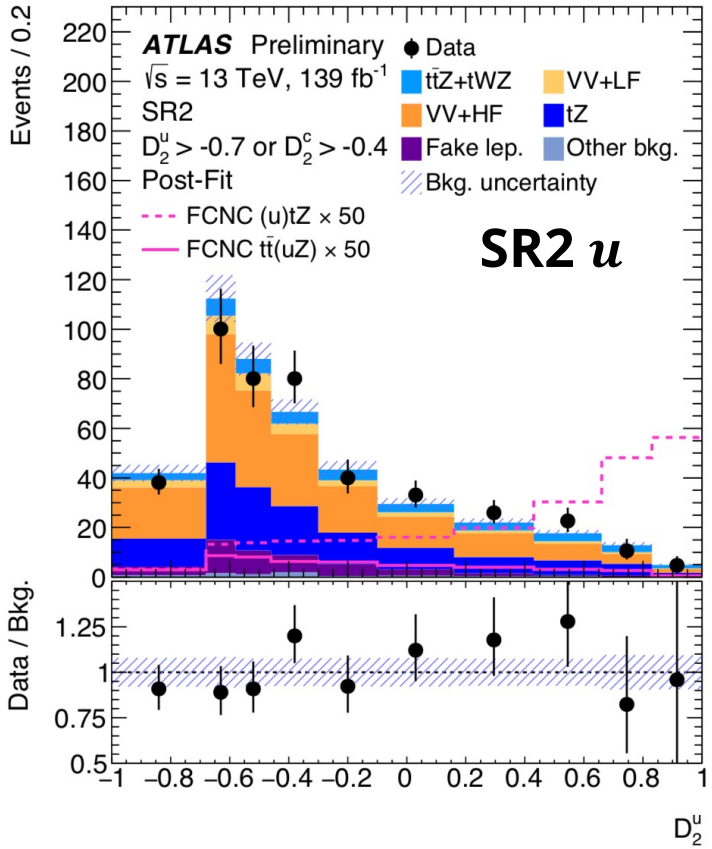

Production mode

- **Stat. and syst. Uncertainties**
  - Analysis is dominated by statistical uncertainties
- Previous ATLAS 36fb^{-1} (focus on decay mode) [J. High Energ. Phys. **2018**, 178]
- This results present a **factor ~3 (2) improvement** $u(c)$ with respect to the previous search
- Adding production mode, optimised signal region and analysis strategy, more luminosity (139 fb^{-1})

FCNC $tqH(\tau\tau)$ Analysis Strategy

- Analysis is optimised in both FCNC production and decay modes
- **Event Selection**
  - $= 1$ b-tagged jet (70% WP), $= 0{,}1$ lepton different regions are defined depending on top and tau decays and jet multiplicity
- **Background Estimation**
  - Fake τ main background scale factor estimated in data-MC control regions
    - Sources are $t\bar{t}$ and multi-jet production
- **Signal Extraction**
  - One BDT is trained per-region to discriminate signal from background
    - Uses 12−17 kinematic input variables ($\tau\ p_{\mathrm{T}}, m_{\tau\tau}, m_{bjj}$, …)
  - **Maximum-likelihood fit** to all 7 analysis regions to obtain limits on EFT WC and BRs

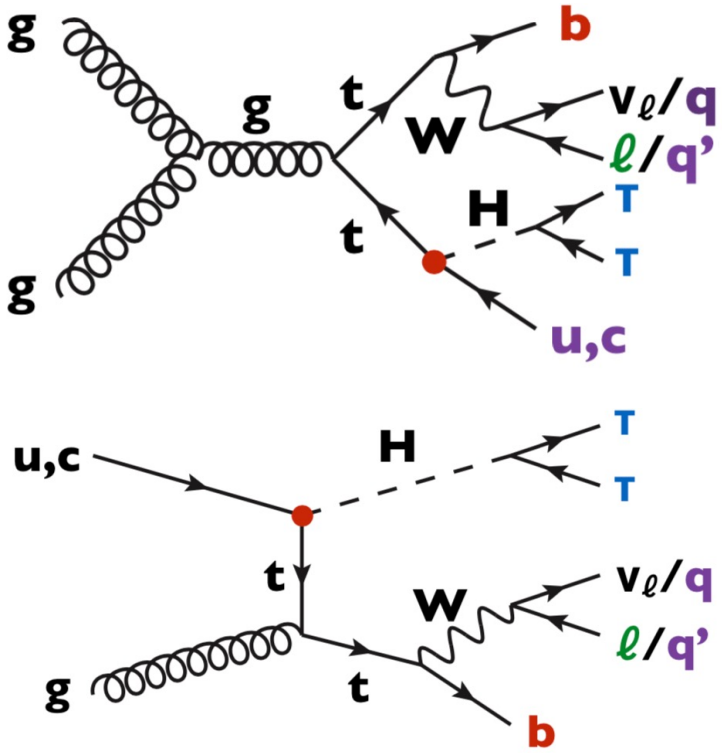

FCNC $tqH(\tau\tau)$ Results

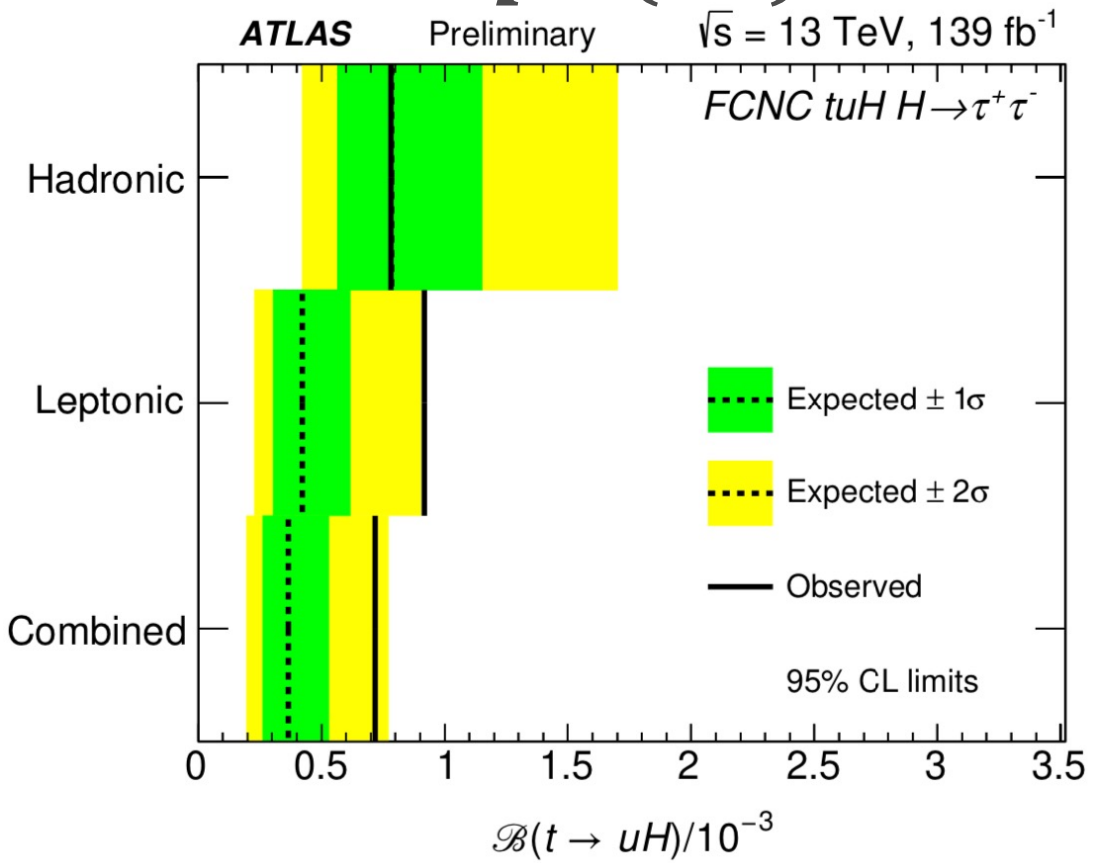

Most sensitive lep region

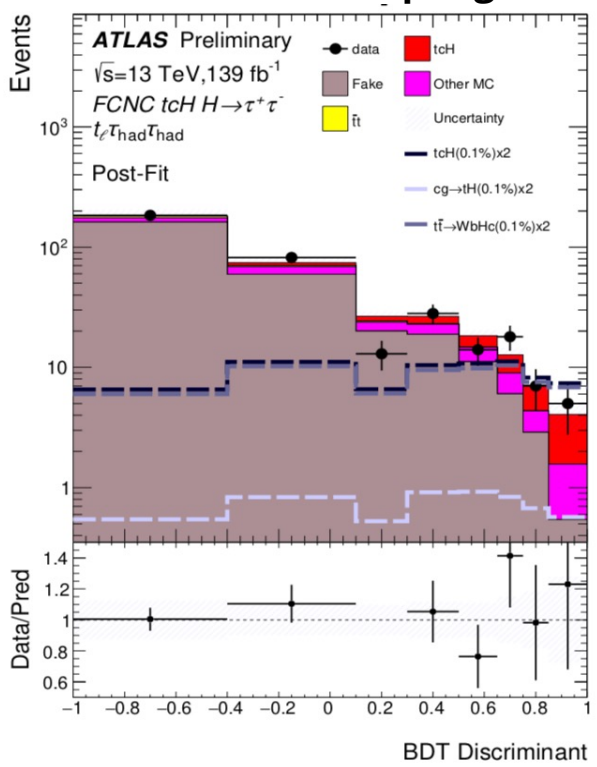

Stat. and syst. uncertainties

- Stat. uncertainties are larger than syst. uncertainties
- MC stats, signal modelling and fake τ modelling are the leading ones
- Observed excess is 2.3σ significant

- Previous ATLAS combination limits ($H \to \tau\tau + bb + \gamma\gamma$ +ML) [J. High Energ. Phys. **2019**, 123]
- This results present a **factor ~1.7 (1.1) improvement** $u(c)$ with respect to the previous combination (factor ~2 wrt. $H \to \tau\tau$ search)
- Optimised signal region and analysis strategy, more luminosity (139 fb-1)

Eur. Phys. J. C **82** (2022) 334

FCNC tqg Analysis Strategy

- Analysis is optimised in FCNC production mode
- Unique single-top signature final state
- **Event selection**
  - $= 1$ central lepton, $= 1$ b-tagged jet (SR) (30% WP), $E_{\mathrm{T}}^{\mathrm{miss}} > 30$ GeV, $m_{l\nu} > 50$ GeV
- **Background Estimation**
  - Validation regions are defined for the main backgrounds: $t\bar{t} + Wt$, W + jets and single-top production
  - Multi-jet background estimation is performed using matrix method
- **Signal Extraction**
  - Two NNs are trained separately for tcg and tug (D_1 and D_2)
    - Uses several kinematic input variables (b-jet p_{T}, m_{lb}, m_{lvb}, ...)
  - **Maximum-likelihood fit** to the signal region to obtain limits on EFT WC and BRs

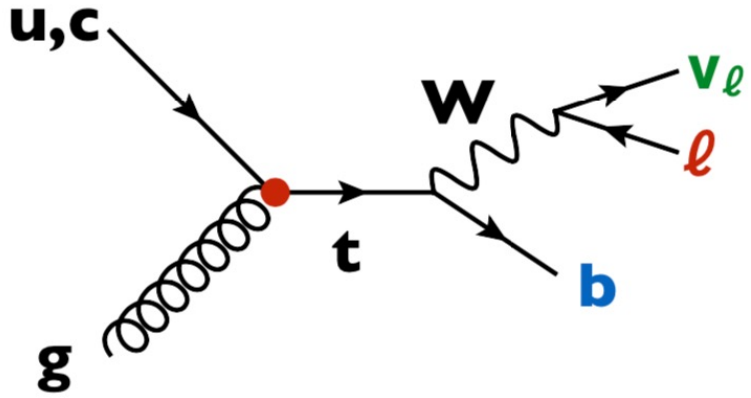

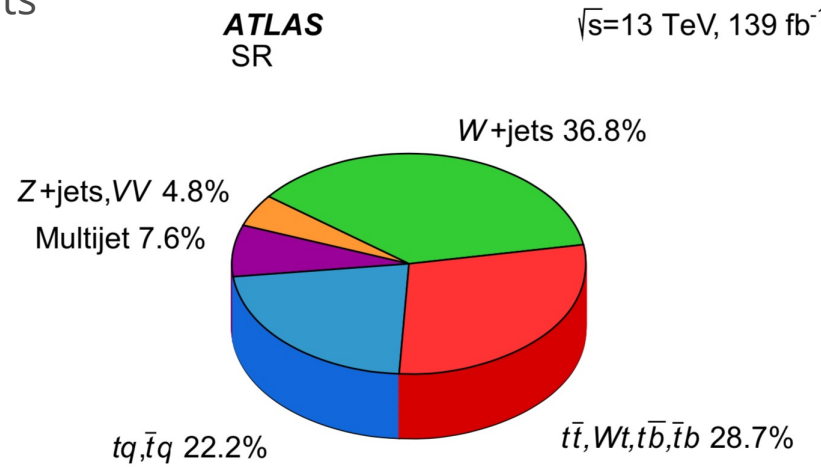

FCNC tqg Results

Eur. Phys. J. C **82** (2022) 334

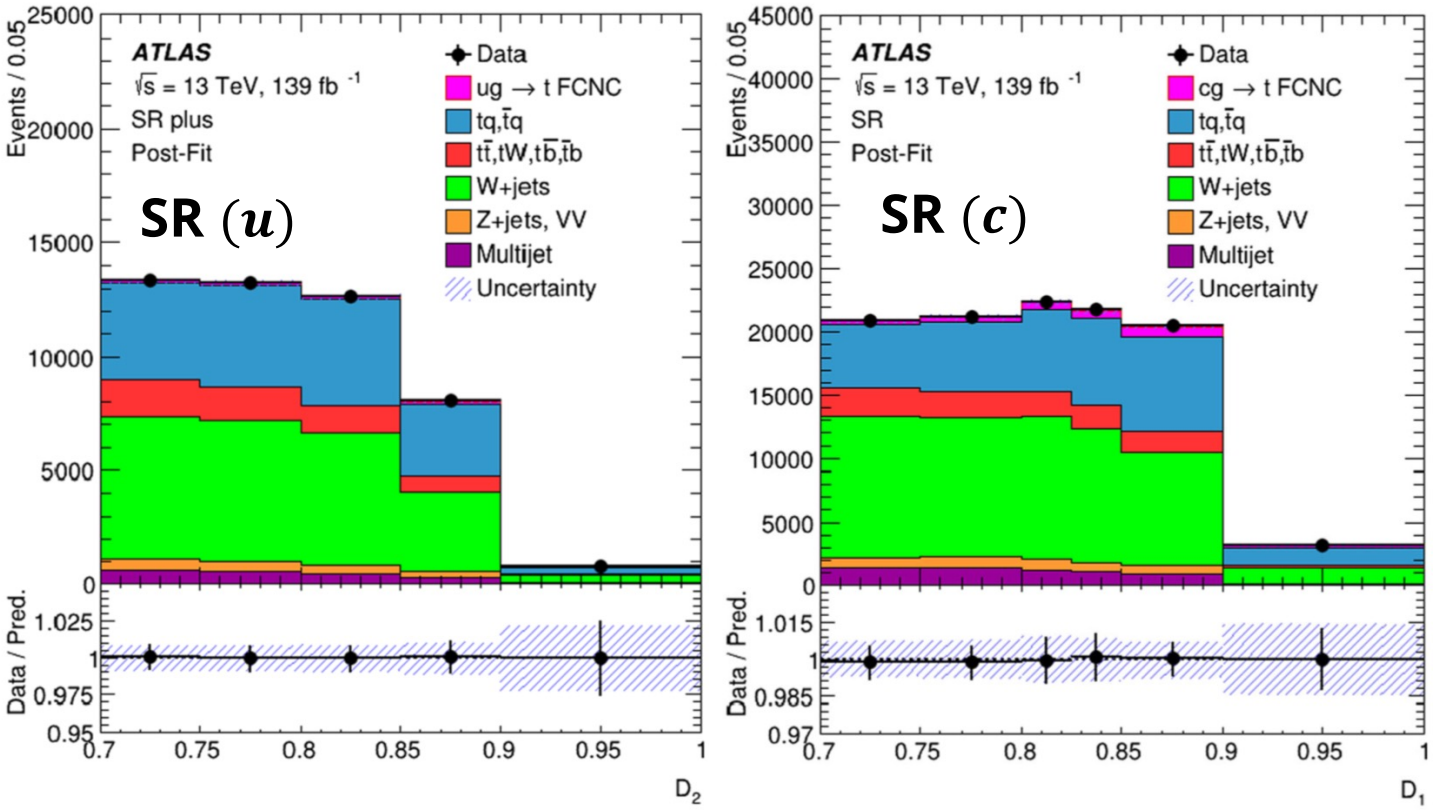

Expected limits

Description	$\mathcal{B}_{95}^{\text{exp}}(t \to u + g)$	$\mathcal{B}_{95}^{\text{exp}}(t \to c + g)$
Data statistical only	1.1×10^{-5}	2.4×10^{-5}
Experimental uncertainties also	3.1×10^{-5}	12×10^{-5}
All uncertainties except MC statistical	3.9×10^{-5}	18×10^{-5}
All uncertainties	4.9×10^{-5}	20×10^{-5}

Stat. and syst. uncertainties

- Addition of all systematics increase limits by factor ~5 (tuZ) and ~10 (tcZ)
- Main uncertainties: bkg. modelling, jet and $E_{\text{T}}^{\text{miss}}$

- This results present a **factor ~2 improvement** with respect to the previous ATLAS Run1 search
- Optimised signal region and analysis strategy, more luminosity (139 fb^{-1})

FCNC Overview

ATL-PHYS-PUB-2022-015

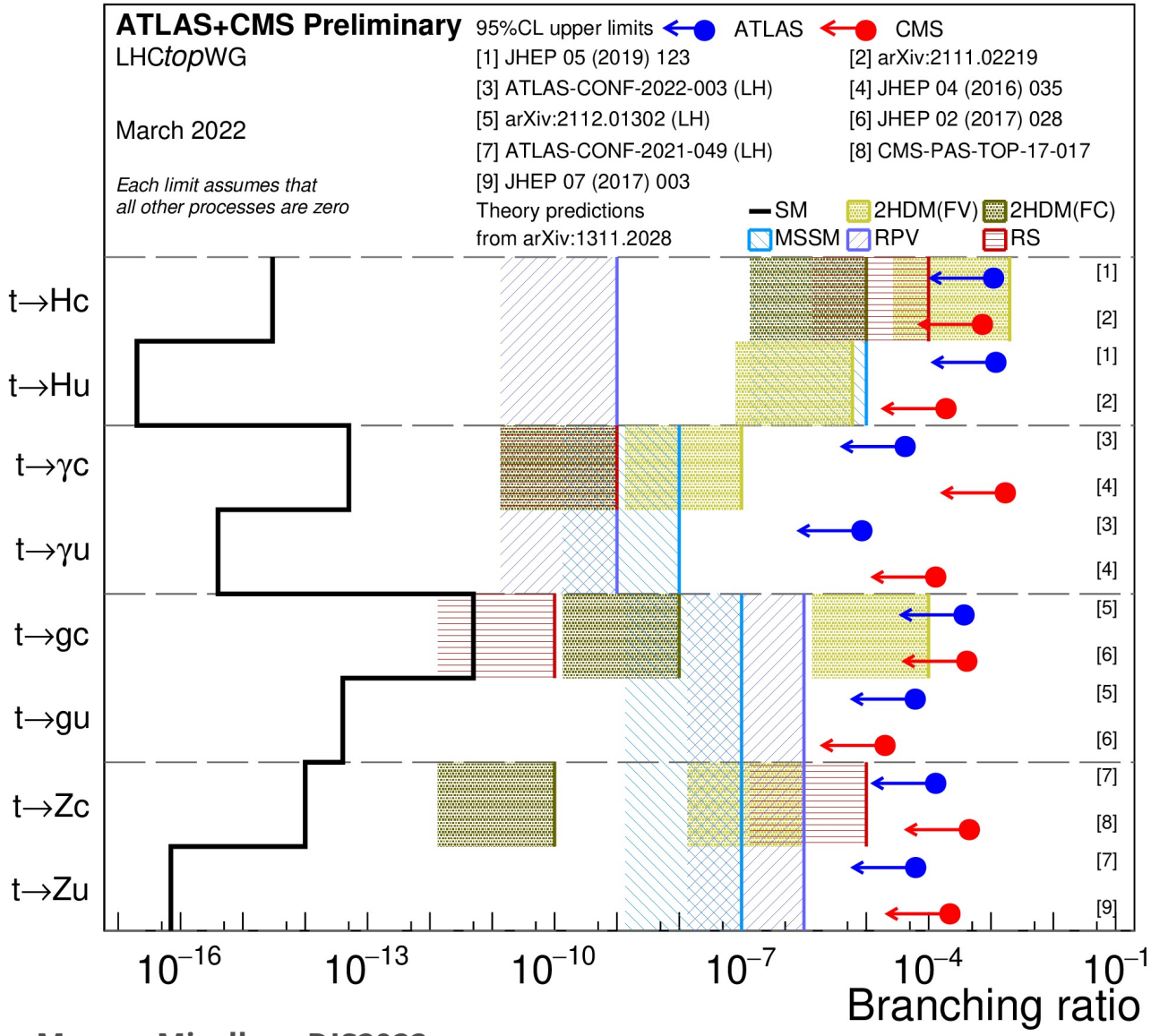

$\sqrt{s} = 13$ TeV, Run2

$\sqrt{s} = 13$ TeV, 36fb^{-1}

$\sqrt{s} = 7 + 8$ TeV, Run1

$\sqrt{s} = 8$ TeV, Run1

	ATLAS (LH)	CMS
	Observed (expected) limits on BR $\times 10^{-5}$	
t→Hc	$\tau\tau$: 99 (50)	$\gamma\gamma$: 73 (51)
t→Hu	$\tau\tau$: 72 (36)	$\gamma\gamma$: 19 (31)
t→γc	4.2 (3.4)	170 (200)
t→γu	0.85 (0.88)	13 (19)
t→gc	37 (20)	41 (28)
t→gu	6.1 (4.9)	2.0 (2.8)
t→Zc	13 (11)	45 (37)
t→Zu	6.2 (4.9)	22 (27)

Summary

- The LHC Run2 data is being exploited:
  - Four-top production combination measurement at **4.7σ (2.6σ)**
  - Observation of single top+photon at **9.1σ (6.7σ)**
  - Overall factor $2-5$ improvement in all FCNC channels wrt. to previous ATLAS results.
    - $tq\gamma \rightarrow$ factor **~3.3–5.2**
    - $tqZ \rightarrow$ factor **~2–3**
    - $tqH \rightarrow$ factor **~1.1–1.7** (big data excess)
    - $tqg \rightarrow$ factor **~2** (syst. dominated)
    - Most of these analysis are stat. dominated → improvement in Run3

- ATLAS Top Physics Results

Back-Up

4tops SRs

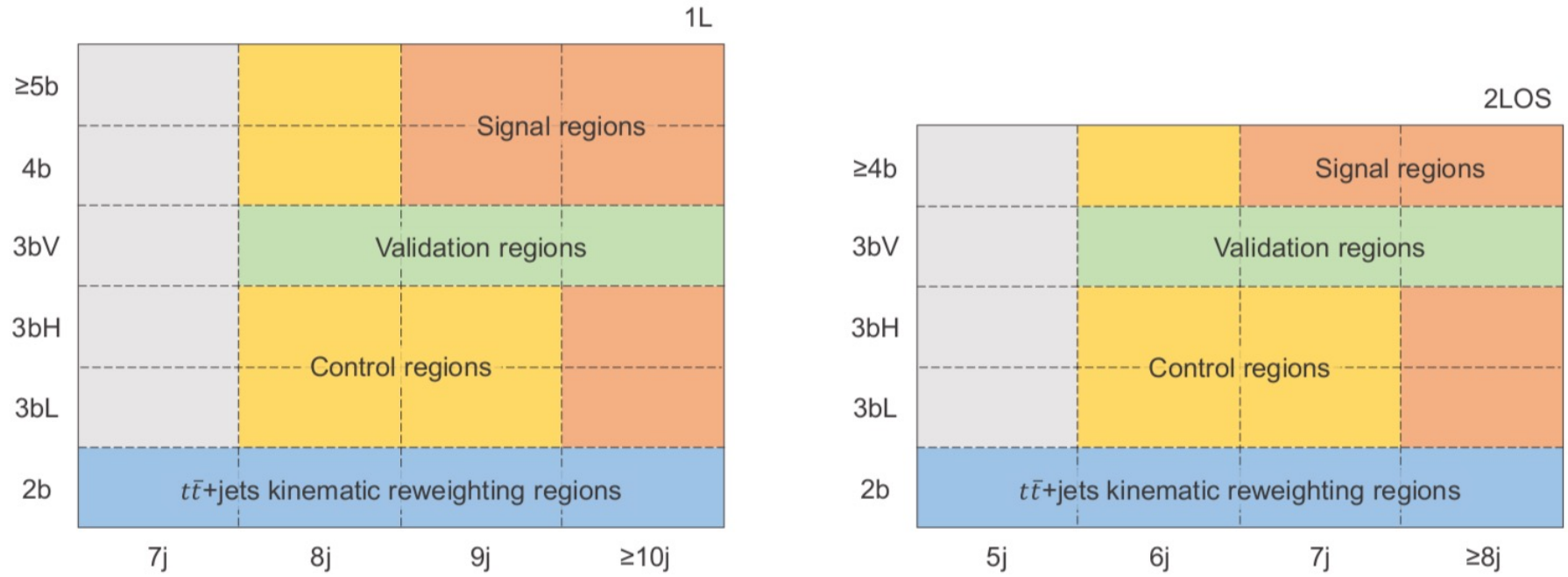

Figure 2. Schematic view of the event categories used to select analysis regions (signal, control, validation and tt+jets reweighting regions) in the 1L channel (left) and 2LOS channel (right). The axes represent the jet multiplicity and *b*-tagging requirements defined in table 1. The 3bL (3bH) *b*-tagging requirement selects events with lower (higher) purity of MC 'truth' *b*-jets amongst the three jets tagged at the 70% OP. The 3bV *b*-tagging requirement is used to define the validation regions. The regions in grey are not used in the analysis.

4tops SRs

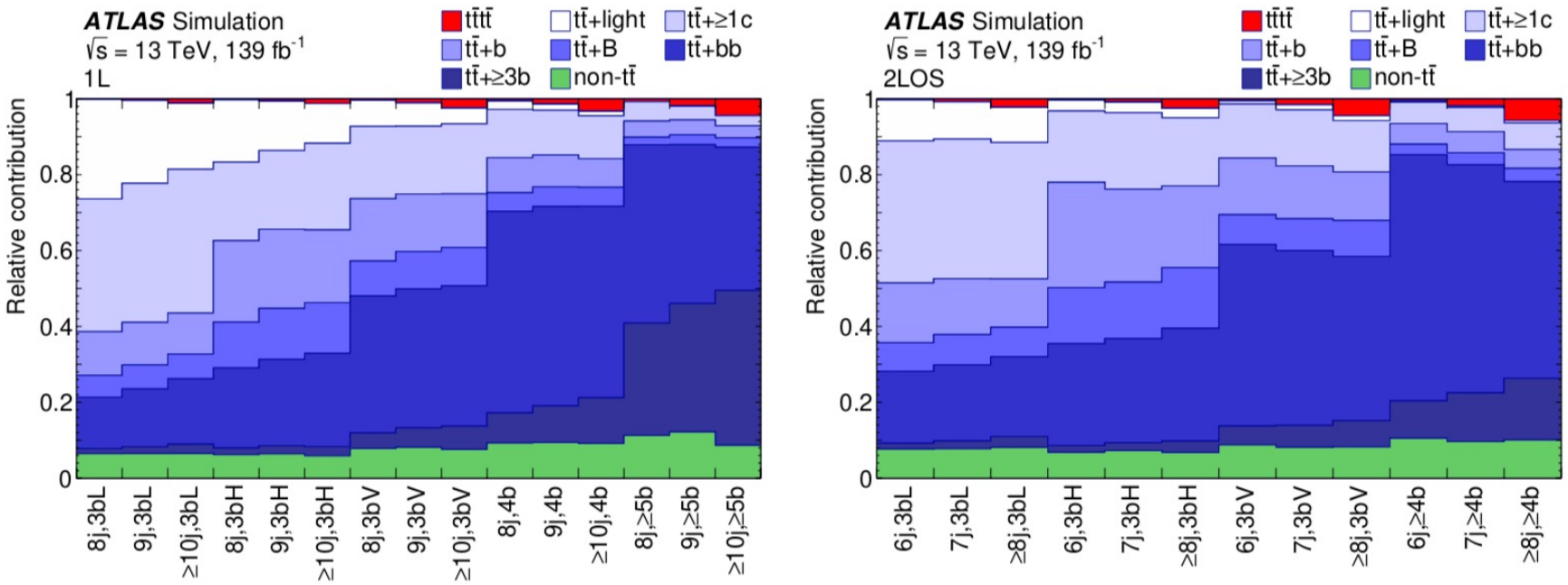

Figure 3. Relative contribution from the signal and backgrounds in all signal, control and validation regions in the 1L channel (left) and 2LOS channel (right). The 3bL (3bH) b-tagging requirement selects events with lower (higher) purity of MC 'truth' b-jets amongst the three jets tagged at the 70% OP. The 3bV b-tagging requirement is used to define the validation regions. For the $t\bar{t}$+jets background, the fraction is shown for each component with the finer classification. The $t\bar{t}t\bar{t}$ signal is normalised to the SM cross-section prediction.

4tops SRs

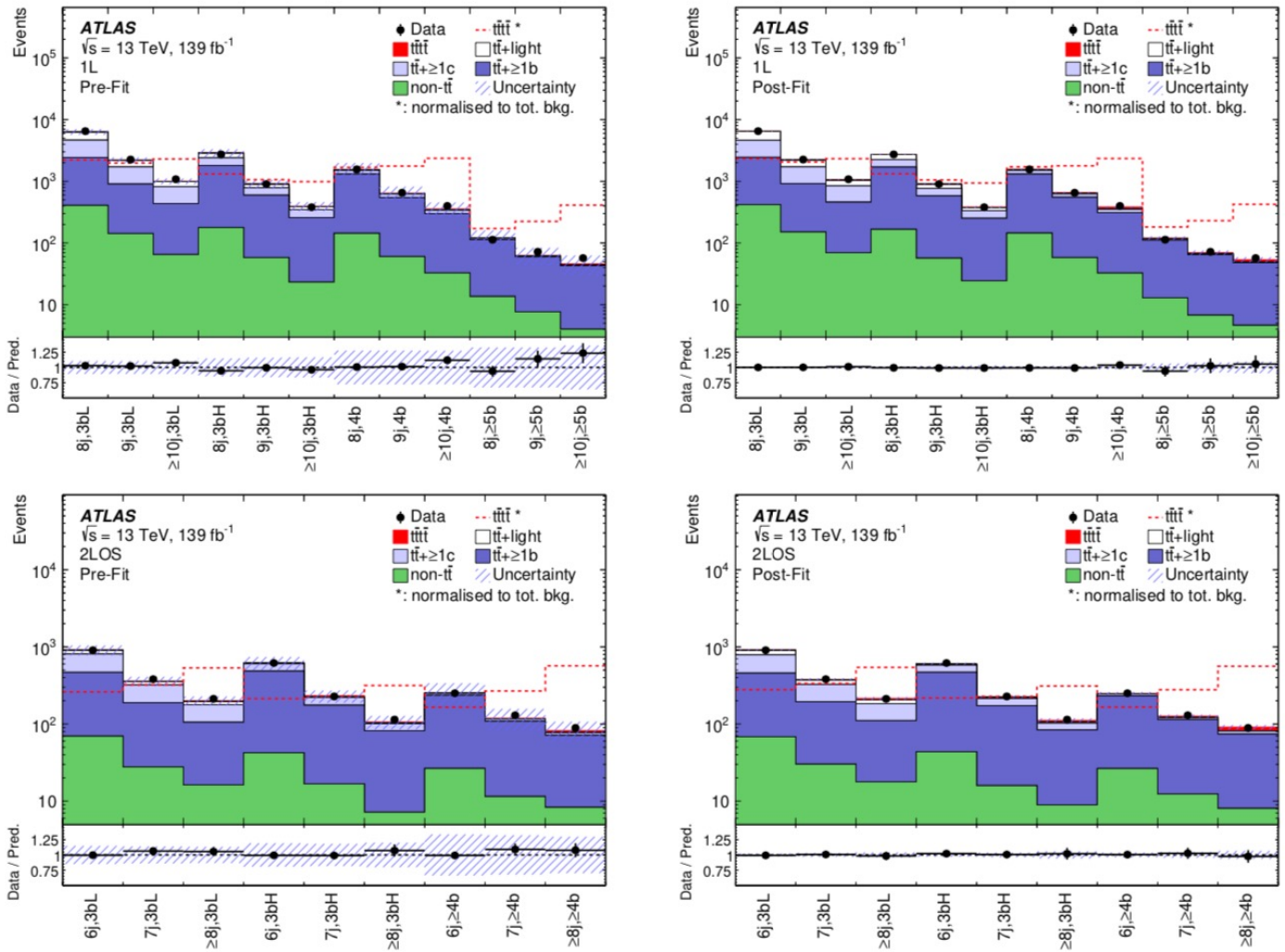

Figure 6. Comparison of predicted and observed event yields in each control and signal region in the 1L channel (top) and in the 2LOS channel (bottom) before the fit (left) and after the fit (right). The $t\bar{t}$+jets background is corrected at the pre-fit level using data. The band includes the total pre- or post-fit uncertainties. The dashed red line shows the signal distribution normalised to the total background yield. The ratio of the data to the total pre- or post-fit prediction is shown in the lower panel.

4tops tt+jets backgound corrections

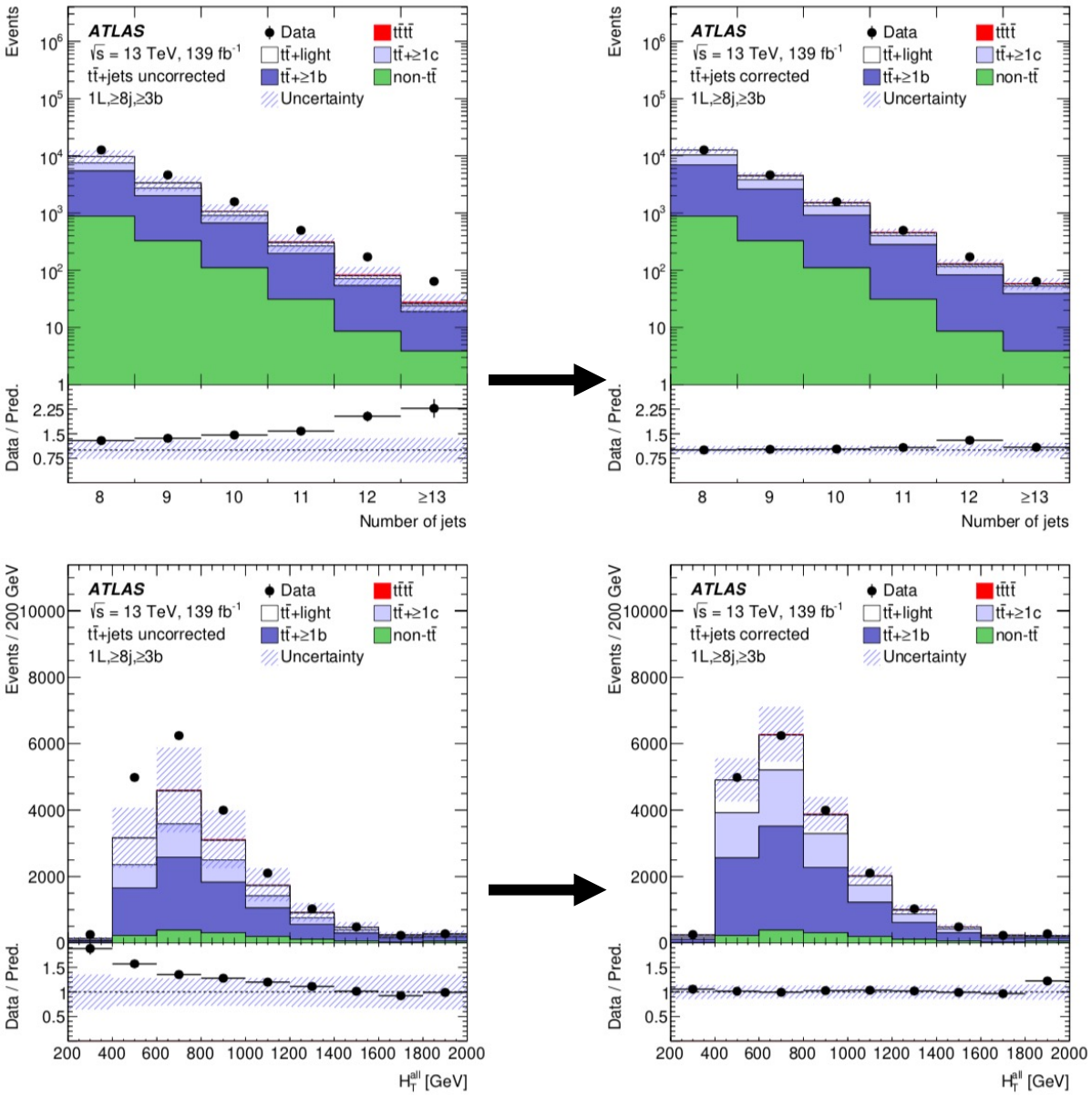

Figure 4. The N_{jets} and $H_{\text{T}}^{\text{all}}$ distributions in the region with ≥ 8 jets and ≥ 3 b-jets in the 1L channel before (left) and after (right) the flavour rescaling and the sequential kinematic reweighting. The band includes the total pre-fit uncertainty of the MC prediction. The ratio of the data to the total MC expectation is shown in the lower panel. The last bin in all distributions includes the overflow.

4tops BDT input variables

- **Overall activity in the transverse plan:** $t\bar{t}t\bar{t}$ production leads to central collision with a more important transverse activity compared to $t\bar{t}$+jets.
  - H_T using all reconstruced jets and leptons in the event,
  - Centrality $\sum_i p_{\mathrm{T}i} / \sum_i E_i$, where the sum includes all reconstruced jets and leptons in the events,
  - Transverse momentum (p_{T}) of the leading jet.
- ***b*-tagging information:** $t\bar{t}t\bar{t}$ production leads to more energetic b-jets with respect to $t\bar{t}$+jets, where additional (b-tagged) jets come from radiations. The b-tagging operating point used for these variables is defined as MV2c10 70%.
  - Minimum ΔR among all pairs of b-tagged jet and lepton,
  - Minimum ΔR among all pairs of b-tagged jets,
  - Sum of the pseudo continuous b-tagging score ($\sum_{i=0}^{i<6} pcb_i$) (see Section 4.4) of the six leading jets ranked in MV2c10 score,
- $\boldsymbol{E_{\mathrm{T}}^{\mathrm{miss}}}$ **and lepton informations:** this last set of variable attemps to probe the W-boson from top-quark decay, which should be more transverse in $t\bar{t}t\bar{t}$ than in $t\bar{t}$+jets.
  - Missing transverse momentum $E_{\mathrm{T}}^{\mathrm{miss}}$
  - For the 1L channel only: W reconstructed transverse mass $m_T(\ell, E_{\mathrm{T}}^{\mathrm{miss}})$
- **Jets information:** $t\bar{t}t\bar{t}$ production leads to more energetic jets with respect to $t\bar{t}$+jets for the same reason as above, and the radiation structure can be exploited using jet-to-jet correlations (*e.g.* $g \to q\bar{q}$ would lead to close jets with a low invariant mass).
  - For the $\geq$10(8)j region in the 1L(OS) channel: jet multiplicity N_{jets},
  - Average ΔR across all pairs of jets,
  - The invariant mass of the triplet of jets that has the minimum ΔR,[9]
- **RC-jets information:** since $t\bar{t}t\bar{t}$ leads to more transverse objects, some of the produced top-quarks could be boosted enough to be contained in a large-R re-clustered jets (see Section 4.3), with a the sub-structure which can help reducing $t\bar{t}$+jets producing less of these boosted topology.
  - Number of RC-jets with a mass higher than 100 GeV,
  - Sum of the first k_t splitting scale d_{12} of all RC-jets[10],
  - Sum of the second k_t splitting scale d_{23} of all RC-jets,

4tops systematic modelling

Uncertainty source	Description	Components (number)
$t\bar{t}$+≥1b normalisation	±50%	$t\bar{t}$+b, $t\bar{t}$+$b\bar{b}$, $t\bar{t}$+B, $t\bar{t}$+≥3b (4)
$t\bar{t}$+≥1c normalisation	±50%	$t\bar{t}$+≥1c (1)
Generator choice	POWHEG vs MadGraph5_aMC@NLO	($t\bar{t}$+light, $t\bar{t}$+≥1c, $t\bar{t}$+b, $t\bar{t}$+$b\bar{b}$, $t\bar{t}$+B, $t\bar{t}$+≥3b) ⊗ (shape, migration) (12)
PS choice	PYTHIA 8 vs HERWIG 7	($t\bar{t}$+light, $t\bar{t}$+≥1c, $t\bar{t}$+b, $t\bar{t}$+$b\bar{b}$, $t\bar{t}$+B, $t\bar{t}$+≥3b) ⊗ (shape, migration) (12)
Renormalisation scale	Varying μ_r in POWHEG	$t\bar{t}$+light, $t\bar{t}$+≥1c, $t\bar{t}$+≥1b (3)
Factorisation scale	Varying μ_f in POWHEG	$t\bar{t}$+light, $t\bar{t}$+≥1c, $t\bar{t}$+≥1b (3)
ISR	Varying α_S^{ISR}(PS) in PYTHIA 8	$t\bar{t}$+light, $t\bar{t}$+≥1c, $t\bar{t}$+≥1b (3)
FSR	Varying μ_f (PS) in PYTHIA 8	$t\bar{t}$+light, $t\bar{t}$+≥1c, $t\bar{t}$+≥1b (3)
5FS vs 4FS	POWHEGBOXRES (4FS) vs POWHEGBOX (5FS)	$t\bar{t}$+b, $t\bar{t}$+$b\bar{b}$, $t\bar{t}$+B, $t\bar{t}$+≥3b (4)

Table 2. Summary of the sources of systematic uncertainty for the $t\bar{t}$+jets modelling. The last column of the table lists the uncorrelated components of each systematic uncertainty source. All systematic uncertainty sources are treated as uncorrelated across the $t\bar{t}$+jets components. For generator and PS choices, each $t\bar{t}$+jets component is further decomposed into a shape component and a migration component. The number of uncorrelated components for each physics source is shown in parentheses.

4tops systematic modelling

Uncertainty source	$\Delta\sigma_{t\bar{t}t\bar{t}}$ [fb]	
Signal Modelling		
$t\bar{t}t\bar{t}$ modelling	+8	−3
Background Modelling		
$t\bar{t}$+≥1b modelling	+8	−7
$t\bar{t}$+≥1c modelling	+5	−4
$t\bar{t}$+jets reweighting	+4	−3
Other background modelling	+4	−3
$t\bar{t}$+light modelling	+2	−2
Experimental		
Jet energy scale and resolution	+6	−4
b-tagging efficiency and mis-tag rates	+4	−3
MC statistical uncertainties	+2	−2
Luminosity	< 1	
Other uncertainties	< 1	
Total systematic uncertainty	+15	−12
Statistical uncertainty	+8	−8
Total uncertainty	+17	−15

4tops BDT discriminants

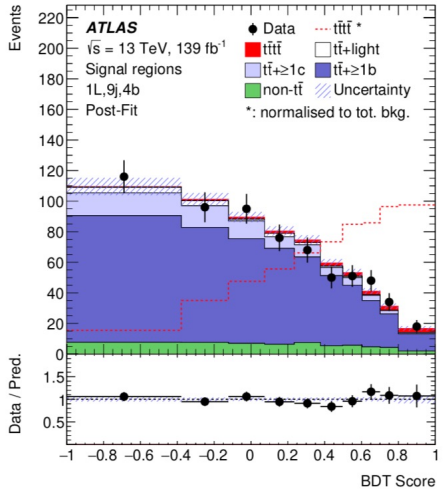

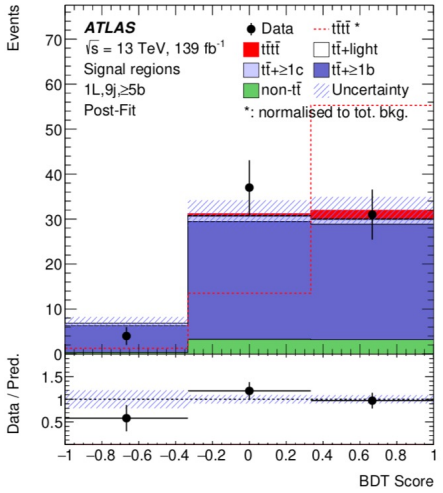

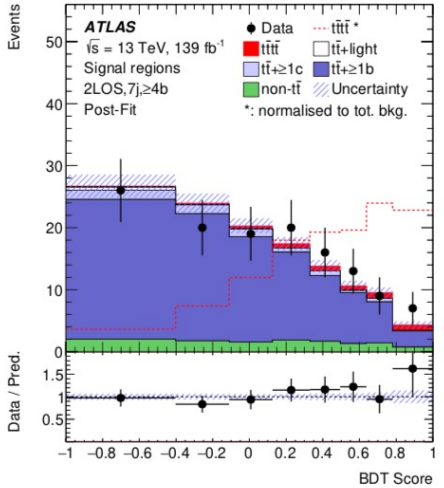

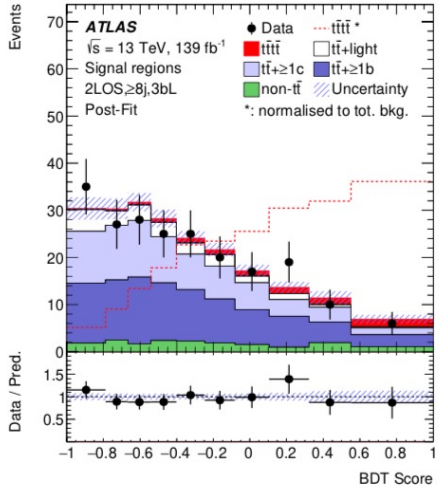

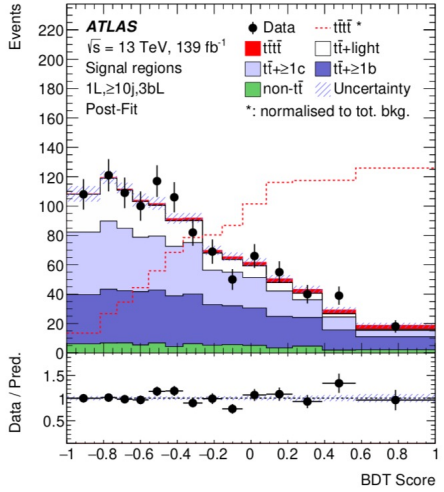

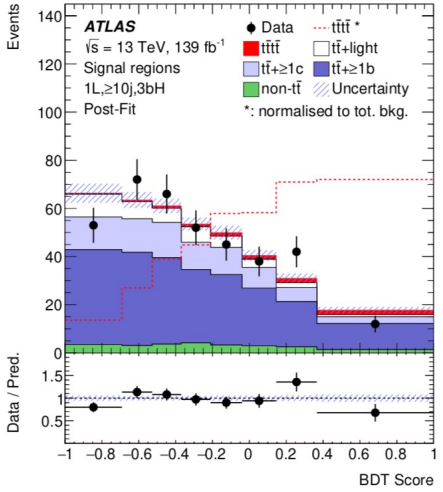

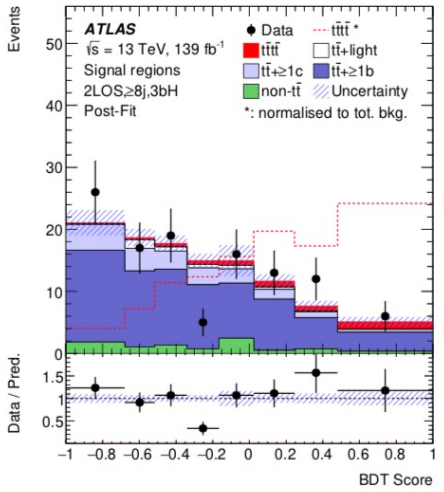

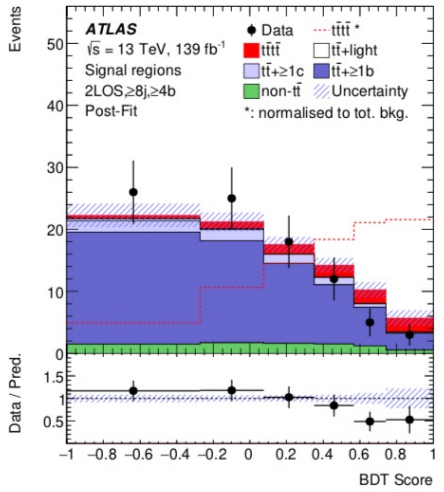

1L

2LOS

FCNC $tq\gamma$ Regions

Table 1: Summary of the analysis region definitions. While the requirements on photons, leptons and $E_{\mathrm{T}}^{\mathrm{miss}}$ are equal, the regions differ by the jet and b-tagged jet requirements. The latter ensure the orthogonality. All jets that pass the 60% b-tagging WP automatically pass the looser b-tagging WPs. A hyphen is set where no criterion has to be fulfilled.

Object	SR	CR $t\bar{t}\gamma$	CR $W\gamma$+jets
Photon		$= 1$	
Lepton		$= 1$	
$E_{\mathrm{T}}^{\mathrm{miss}}$		> 30 GeV	
Jets	≥ 1	≥ 4	≥ 1
b-tagged jets (60% WP)	$= 1$	–	$= 0$
b-tagged jets (70% WP)	$= 1$	≥ 1	$= 0$
b-tagged jets (77% WP)	$= 1$	≥ 2	$= 1$
$m(e,\gamma)$	–	–	$\notin$[80,100] GeV

FCNC $tq\gamma$ BDT input variables

In the following, 18 low-level variables are considered, containing the transverse momentum p_{T}, the pseudorapidity η and the azimuth angle ϕ of

- the photon (γ),
- the lepton (l),
- the b-tagged jet (b-jet),
- the two leading non-b-tagged jets (jet 2, jet 3),

as well as $E_{\mathrm{T}}^{\mathrm{miss}}$, $\phi(E_{\mathrm{T}}^{\mathrm{miss}})$ and the lepton charge.

As high-level variables, the invariant mass m and the angular distance ΔR in the η–ϕ-plane are considered for each pair of two objects, making up 20 variables in total. The other high-level variables are

- the reconstructed top-quark mass: the invariant mass of the decay products of the top-quark candidate is estimated. Firstly, the momentum of the neutrino along the beam axis $p_{z,\nu}$ is approximated by solving the equation $m(l,\nu) = m_W$ to account for the leptonically decaying W boson. For every mathematically possible solution, $m(b\text{-jet}, l, \nu)$ is evaluated and the value closest to the top quark mass is used,
- the transverse W boson mass $m_{\mathrm{T}}(W) = \sqrt{2\left(p_{\mathrm{T}}(l)E_{\mathrm{T}}^{\mathrm{miss}} - \vec{p}_{\mathrm{T}}(l)\cdot\vec{E}_{\mathrm{T}}^{\mathrm{miss}}\right)}$,
- the sum of the b-tags at the DL1r 85% working point,
- the sum of all transverse momenta H_{T},
- the jet multiplicity of the event,
- the photon conversion as a binary variable, i.e. 1 if the photon candidate is converted in any part of the detector, or 0 if it is unconverted.

Out of **44** input variables considered, **37** are used as the input to the NN: these were selected by removing the input variables with **negligible impact** on the separation power of the final discriminant

FCNC $tq\gamma$ Wilson Coefficients

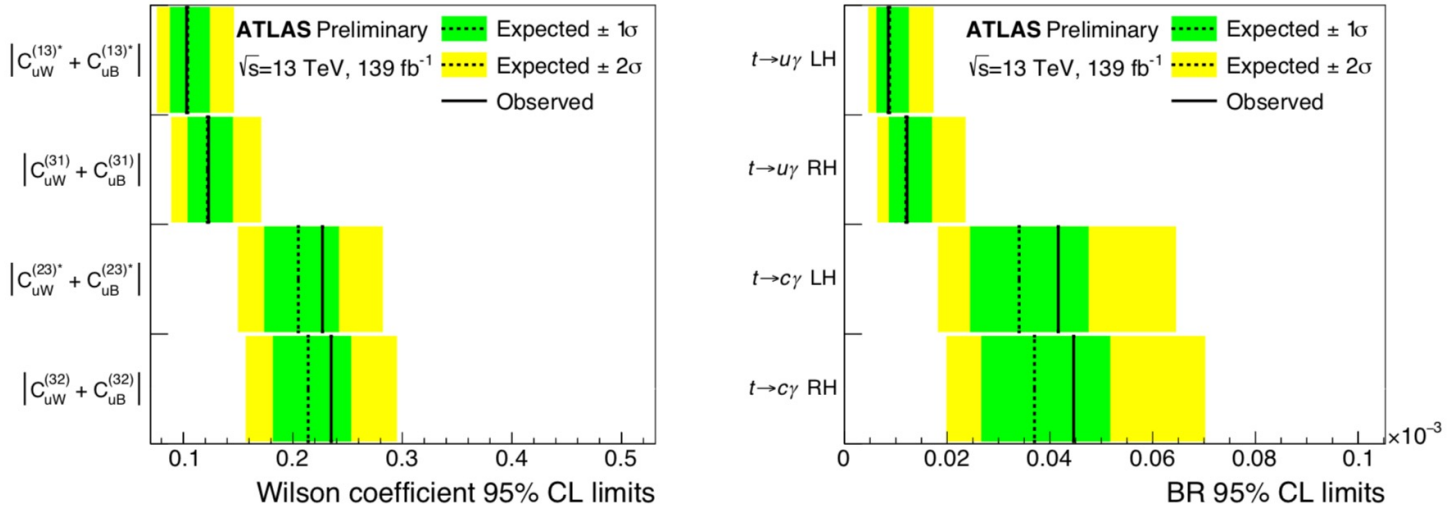

Figure 5: The 95% CL limits on the effective coupling constants (left) and BRs (right). The expected (observed) limits are shown with the dotted (solid) lines. The green (yellow) bands represent one (two) standard deviations for the limits. The scale of new physics is set to $\Lambda = 1$ TeV.

Table 2: The 95% CL limits on the effective coupling constants and BRs. The expected limits with their uncertainties, representing one standard deviation, as well as observed limits are shown. The scale of new physics is set to $\Lambda = 1$ TeV.

Effective coupling	Coefficient limits		Coupling	BRs $[10^{-5}]$	
	Expected	Observed		Expected	Observed
$\lvert C_{uW}^{(13)*} + C_{uB}^{(13)*}\rvert$	$0.104^{+0.020}_{-0.016}$	0.103	$t \to u\gamma$ LH	$0.88^{+0.37}_{-0.25}$	0.85
$\lvert C_{uW}^{(31)} + C_{uB}^{(31)}\rvert$	$0.122^{+0.023}_{-0.018}$	0.123	$t \to u\gamma$ RH	$1.20^{+0.50}_{-0.33}$	1.22
$\lvert C_{uW}^{(23)*} + C_{uB}^{(23)*}\rvert$	$0.205^{+0.037}_{-0.031}$	0.227	$t \to c\gamma$ LH	$3.40^{+1.35}_{-0.95}$	4.16
$\lvert C_{uW}^{(32)} + C_{uB}^{(32)}\rvert$	$0.214^{+0.039}_{-0.032}$	0.235	$t \to c\gamma$ RH	$3.70^{+1.47}_{-1.03}$	4.46

FCNC tqZ χ^2 minimisation and SRs

$$\chi^2_{t\bar{t}} = \frac{\left(m^{\text{reco}}_{j_a\ell\ell} - m_{t_{\text{FCNC}}}\right)^2}{\sigma^2_{t_{\text{FCNC}}}} + \frac{\left(m^{\text{reco}}_{j_b\ell_W\nu} - m_{t_{\text{SM}}}\right)^2}{\sigma^2_{t_{\text{SM}}}} + \frac{\left(m^{\text{reco}}_{\ell_W\nu} - m_W\right)^2}{\sigma^2_W},$$

Table 2: Overview of the requirements applied for selecting events in the signal regions. OSSF is an opposite-sign same-flavor lepton pair. $m_Z = 91.2$ GeV and $m_t = 172.5$ GeV.

Common selections		
Exactly 3 leptons with $p_{\text{T}}(\ell_1) > 27$ GeV ≥ 1 OSSF pair, with $\lvert m_{\ell\ell} - m_Z\rvert < 15$ GeV		
SR1	SR2	
≥ 2 jets	1 jet	2 jets
1 b-jet	1 b-jet	1 b-jet
–	$m_{\text{T}}(\ell_W, \nu) > 40$ GeV	$m_{\text{T}}(\ell_W, \nu) > 40$ GeV
$\lvert m^{\text{reco}}_{j_a\ell\ell} - m_t\rvert < 2\sigma_{t_{\text{FCNC}}}$	–	$\lvert m^{\text{reco}}_{j_a\ell\ell} - m_t\rvert > 2\sigma_{t_{\text{FCNC}}}$
–	$\lvert m^{\text{reco}}_{j_b\ell_W\nu} - m_t\rvert < 2\sigma_{t_{\text{SM}}}$	$\lvert m^{\text{reco}}_{j_b\ell_W\nu} - m_t\rvert < 2\sigma_{t_{\text{SM}}}$

FCNC tqZ BDT input variables

Table 10: Set of variables used in the training of the GBDT in full SR1 to build the D_1 discriminant used in both tZu and tZc couplings searches. Variables are ordered by the separation $\langle s^2 \rangle$ value.

Variable	$\langle s^2 \rangle$	Definition
$m_{b\ell\nu}$	0.1364	SM top-quark candidate mass
p_{T}^{q}	0.07345	u/c-quark candidate transverse momentum
N_{jets}	0.05747	Jet multiplicity
$m_{q\ell\ell}$	0.04173	FCNC top-quark candidate mass
$\Delta R(t_{\mathrm{SM}}, t_{\mathrm{FCNC}})$	0.04109	ΔR between SM and FCNC top-quark candidates
$\Delta R(\ell, Z)$	0.02441	ΔR between W boson lepton and Z boson candidates

Table 11: Set of variables used in the training of the GBDT in full SR2 to build the D_2^u discriminant. Variables are ordered by the separation $\langle s^2 \rangle$ value.

Variable	$\langle s^2 \rangle$	Definition
p_{T}^{Z}	0.3104	Z boson candidate transverse momentum
p_{T}^{b}	0.175	b-quark candidate transverse momentum
$\Delta R(b, Z)$	0.08017	ΔR between b-quark and Z boson candidates
$m_{b\ell\nu}$	0.04636	SM top-quark candidate mass
χ^2_{tZ}	0.03171	χ^2 from the kinematic fit under the tZ production signal hypothesis
$\Delta R(\ell, Z)$	0.024	ΔR between W boson lepton and Z boson candidates

Table 12: Set of variables used in the training of the GBDT in full SR2 to build the D_2^c discriminant. Variables are ordered by the separation $\langle s^2 \rangle$ value.

Variable	$\langle s^2 \rangle$	Definition
p_{T}^{Z}	0.07408	Z boson candidate transverse momentum
p_{T}^{b}	0.05261	b-quark candidate transverse momentum
$m_{b\ell\nu}$	0.02282	SM top-quark candidate mass
$\Delta R(b, Z)$	0.02143	ΔR between b-quark and Z boson candidates
χ^2_{tZ}	0.01561	χ^2 from the kinematic fit under the FCNC tZ production signal hypothesis
$\Delta R(\ell, Z)$	0.008783	ΔR between W boson lepton and Z boson candidates

FCNC tqZ Control Regions

Table 3: Overview of the requirements applied for selecting events in the control regions. OSSF is an opposite-sign same-flavor lepton pair. $m_Z = 91.2$ GeV and $m_t = 172.5$ GeV.

Common selections			
Exactly 3 leptons with $p_{\mathrm{T}}(\ell_1) > 27$ GeV			
$t\bar{t}$ CR	$t\bar{t}Z$ CR	Side-band CR1	Side-band CR2
≥ 1 OS pair, no OSSF	≥ 1 OSSF pair with $\lvert m_{\ell\ell} - m_Z \rvert < 15$ GeV	≥ 1 OSSF pair with $\lvert m_{\ell\ell} - m_Z \rvert < 15$ GeV	≥ 1 OSSF pair with $\lvert m_{\ell\ell} - m_Z \rvert < 15$ GeV
–	–	–	$m_{\mathrm{T}}(\ell_W, \nu) > 40$ GeV
≥ 1 jet	≥ 4 jets	≥ 2 jets	1 jet
1 b-jet	2 b-jets	1 b-jet	1 b-jet
–	–	$\lvert m^{\mathrm{reco}}_{j_a \ell\ell} - m_t \rvert > 2\sigma_{t_{\mathrm{FCNC}}}$	–
–	–	$\lvert m^{\mathrm{reco}}_{j_b \ell_W \nu} - m_t \rvert > 2\sigma_{t_{\mathrm{SM}}}$	$\lvert m^{\mathrm{reco}}_{j_b \ell_W \nu} - m_t \rvert > 2\sigma_{t_{\mathrm{SM}}}$

FCNC tqZ Wilson Coefficients

Table 7: Observed and expected 95% CL limits on the FCNC $t \to Zq$ branching ratios and the effective coupling strengths for different vertices and couplings (bottom eight rows). For the latter, the energy scale is assumed to be $\Lambda_{NP} = 1\,\text{TeV}$. The top rows show, for the case of the FCNC $t \to Zu$ branching ratio, the observed and expected limits 95% CL when only one of the two SRs, either SR1 or SR2, and all CRs are included in the likelihood.

Observable	Vertex	Coupling	Observed	Expected
	SR1+CRs			
$\mathcal{B}(t \to Zq)\ [10^{-5}]$	tZu	LH	9.7	$8.6^{+3.6}_{-2.4}$
$\mathcal{B}(t \to Zq)\ [10^{-5}]$	tZu	RH	9.5	$8.2^{+3.4}_{-2.3}$
	SR2+CRs			
$\mathcal{B}(t \to Zq)\ [10^{-5}]$	tZu	LH	7.8	$6.1^{+2.7}_{-1.7}$
$\mathcal{B}(t \to Zq)\ [10^{-5}]$	tZu	RH	9.0	$6.6^{+2.9}_{-1.8}$
	SRs+CRs			
$\mathcal{B}(t \to Zq)\ [10^{-5}]$	tZu	LH	6.2	$4.9^{+2.1}_{-1.4}$
$\mathcal{B}(t \to Zq)\ [10^{-5}]$	tZu	RH	6.6	$5.1^{+2.1}_{-1.4}$
$\mathcal{B}(t \to Zq)\ [10^{-5}]$	tZc	LH	13	11^{+5}_{-3}
$\mathcal{B}(t \to Zq)\ [10^{-5}]$	tZc	RH	12	10^{+4}_{-3}
$\lvert C_{uW}^{(13)*}\rvert$ and $\lvert C_{uB}^{(13)*}\rvert$	tZu	LH	0.15	$0.13^{+0.03}_{-0.02}$
$\lvert C_{uW}^{(31)}\rvert$ and $\lvert C_{uB}^{(31)}\rvert$	tZu	RH	0.16	$0.14^{+0.03}_{-0.02}$
$\lvert C_{uW}^{(23)*}\rvert$ and $\lvert C_{uB}^{(23)*}\rvert$	tZc	LH	0.22	$0.20^{+0.04}_{-0.03}$
$\lvert C_{uW}^{(32)}\rvert$ and $\lvert C_{uB}^{(32)}\rvert$	tZc	RH	0.21	$0.19^{+0.04}_{-0.03}$

FCNC tqH Previous Results

Table 1: Summary of 95% CL upper limits on $\mathscr{B}(t \to cH)$ and $\mathscr{B}(t \to uH)$ obtained from ATLAS and CMS Collaborations with Run 2 data. Each limit is obtained assuming the other branching ratio is null.

		$\mathcal{L}$ [fb^{-1}]	95% CL observed upper limits on $\mathscr{B}(t \to cH)$	95% CL observed upper limits on $\mathscr{B}(t \to uH)$
ATLAS	$H \to b\bar{b}$ [32]	36.1	4.2×10^{-3}	5.2×10^{-3}
	$H \to \gamma\gamma$ [33]	36.1	2.2×10^{-3}	2.4×10^{-3}
	$H \to \tau\tau$ ($\tau_{\text{lep}}\tau_{\text{had}}$, $\tau_{\text{had}}\tau_{\text{had}}$) [32]	36.1	1.9×10^{-3}	1.7×10^{-3}
	$H \to WW^*, \tau\tau, ZZ^*$ (2ℓSS, 3ℓ) [34]	36.1	1.6×10^{-3}	1.9×10^{-3}
	Combination [32]	36.1	1.1×10^{-3}	1.2×10^{-3}
CMS	$H \to b\bar{b}$ [35]	35.9	4.7×10^{-3}	4.7×10^{-3}
	$H \to b\bar{b}$ [36]	137	9.4×10^{-4}	7.9×10^{-4}

FCNC tqH Selections and Regions

Table 2: Summary of preselection requirements. The leading and subleading τ_{had} candidates are denoted by $\tau_{\text{had},1}$ and $\tau_{\text{had},2}$ respectively.

Requirement	leptonic channel			hadronic channel
	$t_h\tau_{\text{lep}}\tau_{\text{had}}$	$t_\ell\tau_{\text{had}}\tau_{\text{had}}$	$t_\ell\tau_{\text{had}}$	$t_h\tau_{\text{had}}\tau_{\text{had}}$
Trigger	single-lepton trigger			di-τ trigger
Leptons	=1 isolated e or μ			=0 isolated e or μ
τ_{had}	=1 τ_{had}	≥2 τ_{had}	=1 τ_{had}	≥2 τ_{had}
Electric charge (Q)	$Q_\ell \times Q_{\tau_{\text{had},1}} < 0$	$Q_{\tau_{\text{had},1}} \times Q_{\tau_{\text{had},2}} < 0$	$Q_\ell \times Q_{\tau_{\text{had},1}} > 0$	$Q_{\tau_{\text{had},1}} \times Q_{\tau_{\text{had},2}} < 0$
Jets	≥ 3 jets	≥1 jets	≥2 jets	≥3 jets
b-tagging	=1 b-jets			=1 b-jets

Table 4: Overview of the signal regions (SR), validation region (VR), and $t\bar{t}$ control regions (CRtt) used for the fake tau scale factor derivation in the leptonic channels. Leptons are required to have either same-sign (SS) or opposite-sign (OS) in each region.

Regions		b-jet	light flavour jets	lepton	hadronic taus	charge
SR	$t_\ell\tau_{\text{had}}\tau_{\text{had}}$	1	≥ 0	1	2	$\tau_{\text{had}}\tau_{\text{had}}$ OS
	$t_\ell\tau_{\text{had}}$-1j	1	1	1	1	$t_\ell\tau_{\text{had}}$ SS
	$t_\ell\tau_{\text{had}}$-2j	1	2	1	1	$t_\ell\tau_{\text{had}}$ SS
	$t_h\tau_{\text{lep}}\tau_{\text{had}}$-2j	1	2	1	1	$\tau_{\text{lep}}\tau_{\text{had}}$ OS
	$t_h\tau_{\text{lep}}\tau_{\text{had}}$-3j	1	≥ 3	1	1	$\tau_{\text{lep}}\tau_{\text{had}}$ OS
	$t_h\tau_{\text{had}}\tau_{\text{had}}$-2j	1	2	0	2	$\tau_{\text{had}}\tau_{\text{had}}$ OS
	$t_h\tau_{\text{had}}\tau_{\text{had}}$-3j	1	≥ 3	0	2	$\tau_{\text{had}}\tau_{\text{had}}$ OS
VR	$t_\ell\tau_{\text{had}}\tau_{\text{had}}$-SS	1	≥ 0	1	2	$\tau_{\text{had}}\tau_{\text{had}}$ SS
CRtt	$t_\ell t_\ell 1b\tau_{\text{had}}$	1	≥ 0	2	1	$t_\ell t_\ell$ OS
	$t_\ell t_\ell 2b\tau_{\text{had}}$	2	≥ 0	2	1	$t_\ell t_\ell$ OS
	$t_\ell t_h 2b\tau_{\text{had}}$-2jSS	2	2	1	1	$t_\ell\tau_{\text{had}}$ SS
	$t_\ell t_h 2b\tau_{\text{had}}$-2jOS	2	2	1	1	$t_\ell\tau_{\text{had}}$ OS
	$t_\ell t_h 2b\tau_{\text{had}}$-3jSS	2	≥ 3	1	1	$t_\ell\tau_{\text{had}}$ SS
	$t_\ell t_h 2b\tau_{\text{had}}$-3jOS	2	≥ 3	1	1	$t_\ell\tau_{\text{had}}$ OS

FCNC tqH BDT inputs

Table 5: Discriminating variables (n) used in the training of the BDT of each SR. The ranking of the input variables according to their importance in the training is reported from highest (1) to lowest (n). Variables whose ranking is missing are not included in the training of the corresponding SR. The description of each variable is provided in the text.

	$t_l\tau_{\text{had}}$-1j	$t_h\tau_{\text{lep}}\tau_{\text{had}}$-2j	$t_l\tau_{\text{had}}$-2j	$t_h\tau_{\text{lep}}\tau_{\text{had}}$-3j	$t_\ell 2\tau_{\text{had}}$	$t_h 2\tau_{\text{had}}$-2j	$t_h 2\tau_{\text{had}}$-3j
Total variables (n)	12	15	12	17	15	12	12
m_{jj}				9		6	7
χ^2				14			
$\max(\eta_\tau)$	4		4		10		
m_{T}^W	11		8		13		
$m_{\tau\tau,\text{fit}}$		2		3		1	1
$m_{\text{bjj,fit}}$		1		2		3	4
$p_{\text{T}}{}^\ell$	12	15	12	17			
$m_{\tau\tau\text{q,fit}}$						10	6
m_{bjj}	3		5		4		
$p_{\text{T}\tau 1}$	1	4	1	1	5	11	10
$E_{\text{T}}^{\text{miss}}$	5	11	10	13	6	7	13
$m_{\tau\tau}$	10	14	11	6	1	2	2
$E_{\tau 1}/E_{\tau 1,\text{fit}}$		10		12		8	8
$E_{\tau 2}/E_{\tau 2,\text{fit}}$		7		4		9	11
$p_{\text{T}\tau^+\tau^-}$					9		
$m_{\tau\tau\text{q}}$					3		
$\Delta\phi(\tau\tau, E_{\text{T}}^{\text{miss}})$		6		16		13	12
$E_{\text{T}}^{\text{miss}}$centrality		13		15		12	9
$\min(m_{\tau\tau\text{j}})$	9		3		14		
$\min(\Delta R(\ell,\tau))$	8	9	9	10	15		
$\Delta R(\tau,\tau)$					2	4	3
$\Delta R(\ell, b\text{-jet})$	2	3	2	8	12		
$\Delta R(\tau 1, b\text{-jet})$	6	5	6	7	11		
$\Delta R(\ell + b\text{-jet}, \tau\tau)$					7		
$\Delta R(\tau 1, \text{light-jet})$	7	8	7	5	8	5	5
$\min(m_{jj})$		12		11			

FCNC tqH Systematics

Table 7: Absolute uncertainties on $\mathscr{B}(t \to qH)$ $(q = u, c)$ obtained from the combined fit to data. The uncertainties are symmetrised for a presentation purpose and grouped into the categories described in the Section 9.

Source of uncertainty	$\Delta\mathscr{B}$ $[10^{-5}]$	
	$t \to uH$	$t \to cH$
Lepton ID	0.6	1.0
$E_{\mathrm{T}}^{\mathrm{miss}}$	0.7	0.8
Fake lepton modeling	0.9	1.1
JES and JER	2.4	3.2
Flavour tagging	2.7	3.7
$t\bar{t}$ modeling	2.9	4.3
Other MC modeling	2.1	2.9
Fake τ modeling	3.2	4.6
Signal modeling including Br$(H \to \tau\tau)$	5.3	7.0
τ ID	3.3	4.4
Luminosity and Pileup	0.9	1.3
MC statistics	5.1	7.0
Total systematic uncertainty	11.2	15.5
Data statistical uncertainty	14.1	19.6
Total uncertainties	18	25

FCNC tqH Wilson Coefficients

Table 8: Summary of 95% CL upper limits on $\mathscr{B}(t \to cH)$ and $\mathscr{B}(t \to uH)$, significance and best-fit branching ratio in signal regions with a benchmark branching ratio of $\mathscr{B}(t \to qH) = 0.1\%$. Expected significance is obtained from Asimov fit with a signal injection corresponding to a branching ratio of 0.1%.

	$t \to cH$			$t \to uH$		
Signal Regions	95% CL upper limits[10^{-3}] Observed (Expected)	Significance	$\mathscr{B}[10^{-3}]$	95% CL upper limits[10^{-3}] Observed (Expected)	Significance	$\mathscr{B}[10^{-3}]$
$t_h\tau_{had}\tau_{had}$-2j	$1.85(2.80^{+1.30}_{-0.78})$	−0.96(0.78)	$-1.03^{+1.04}_{-1.04}$	$1.10(1.65^{+0.79}_{-0.46})$	−0.90(1.25)	$-0.55^{+0.59}_{-0.59}$
$t_h\tau_{had}\tau_{had}$-3j	$1.18(1.06^{+0.50}_{-0.30})$	0.34(1.87)	$0.16^{+0.47}_{-0.47}$	$1.00(0.89^{+0.42}_{-0.25})$	0.36(2.13)	$0.14^{+0.40}_{-0.40}$
Hadronic Combination	$1.04(0.98^{+0.46}_{-0.28})$	0.26 (1.99)	$0.11^{+0.43}_{-0.43}$	$0.78(0.78^{+0.37}_{-0.22})$	0.11(2.33)	$0.04^{+0.34}_{-0.34}$
$t_l\tau_{had}$-2j	$4.86(4.32^{+1.89}_{-1.21})$	0.40(0.48)	$0.81^{+2.04}_{-2.04}$	$3.93(3.55^{+1.56}_{-0.99})$	0.34(0.58)	$0.57^{+1.66}_{-1.66}$
$t_l\tau_{had}$-1j	$3.94(3.67^{+1.66}_{-1.03})$	0.24(0.57)	$0.40^{+1.70}_{-1.70}$	$3.10(2.87^{+1.29}_{-0.80})$	0.24(0.73)	$0.31^{+1.33}_{-1.33}$
$t_h\tau_{lep}\tau_{had}$-2j	$4.81(5.85^{+2.90}_{-1.63})$	−0.52(0.39)	$-1.36^{+2.56}_{-2.56}$	$2.56(3.05^{+1.38}_{-0.85})$	−0.48(0.69)	$-0.66^{+1.38}_{-1.38}$
$t_h\tau_{lep}\tau_{had}$-3j	$2.78(2.79^{+1.36}_{-0.78})$	−0.04(0.76)	$-0.04^{+1.26}_{-1.26}$	$2.07(2.09^{+0.94}_{-0.58})$	−0.05(0.98)	$-0.04^{+0.98}_{-0.98}$
$t_l\tau_{had}\tau_{had}$	$1.41(0.63^{+0.29}_{-0.18})$	2.64(3.24)	$0.74^{+0.34}_{-0.34}$	$1.01(0.45^{+0.21}_{-0.13})$	2.64(4.08)	$0.53^{+0.25}_{-0.25}$
Leptonic Combination	$1.29(0.59^{+0.27}_{-0.17})$	2.59(3.34)	$0.68^{+0.32}_{-0.32}$	$0.92(0.42^{+0.19}_{-0.12})$	2.59(4.23)	$0.48^{+0.23}_{-0.23}$
Combination	$0.99\ (0.50^{+0.22}_{-0.14})$	2.34(3.69)	$0.51^{+0.25}_{-0.25}$	$0.72\ (0.36^{+0.17}_{-0.10})$	2.31(4.49)	$0.37^{+0.18}_{-0.18}$

FCNC tqH Limits

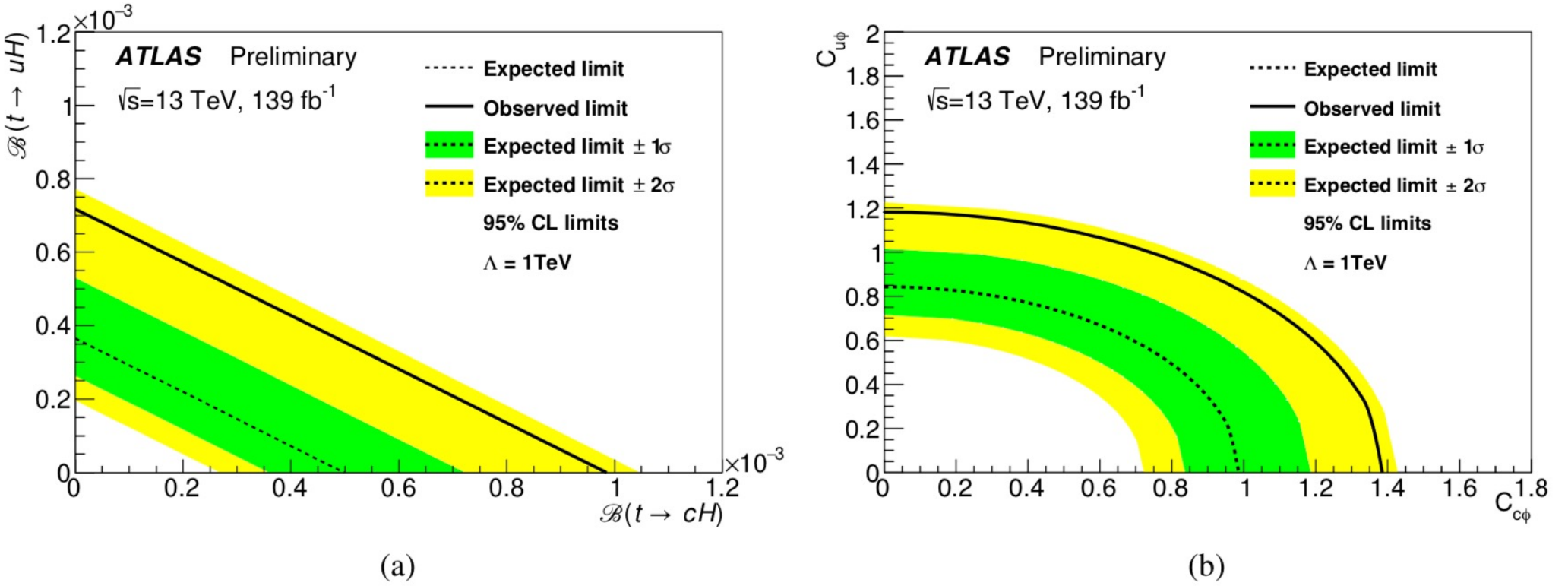

Figure 5: 95% CL upper limits (a) on the plane of $\mathscr{B}(t \to uH)$ versus $\mathscr{B}(t \to cH)$ and (b) on the plane of $C_{c\phi}$ versus $C_{u\phi}$ for the combination of the searches. The observed limits (solid lines) are compared with the expected (median) limits under the background-only hypothesis (dotted lines). The surrounding shaded bands correspond to the 68% and 95% CL intervals around the expected limits, denoted by $\pm 1\sigma$ and $\pm 2\sigma$, respectively.

FCNC tqg Regions

Table 1 Summary of selection requirements used to define the four analysis regions. The left column lists the observables on which the requirements are based. The first part of the table lists requirements which are common to all four analysis regions and define the basic event selection described in Sect. 4.2. Tight electrons and medium muons were counted based on a p_{T} threshold of 27 GeV and they are a subset of the corresponding Loose quality category. Loose charged leptons had to exceed a threshold of $p_{\mathrm{T}}(\ell) = 10\,\mathrm{GeV}$. The transverse mass of the W boson, $m_{\mathrm{T}}(W)$, is defined in Eq. (1). The efficiency of the b-tagging working point used to identify b-jets is denoted by ϵ_b. The symbol D_1 represents one of the NN discriminants defined in Sect. 6

Observable	Common requirements
$n_{\mathrm{Tight}}(e) + n_{\mathrm{Medium}}(\mu)$	$= 1$
$n_{\mathrm{Loose}}(e) + n_{\mathrm{Loose}}(\mu)$	$= 1$
$E_{\mathrm{T}}^{\mathrm{miss}}$	$> 30\,\mathrm{GeV}$
$m_{\mathrm{T}}(W)$	> 50 Gev
$n(j)$	≥ 1
$p_{\mathrm{T}}(\ell)$	$> 50\ \mathrm{Gev} \cdot \left(1 - \frac{\pi - \lvert\Delta\phi(j_1,\ell)\rvert}{\pi - 1}\right)$

	Analysis regions			
	SR	W+jetsVR	$t\bar{t}$ VR	tqVR
$n(\lvert\eta(j)\rvert < 2.5)$	$= 1$	$= 1$	$= 2$	$= 1$
$n(b)$	$= 1$	$= 1$	$= 2$	$= 1$
ϵ_b	30%	60% (veto 30%)	30%	30%
$n(\lvert\eta(j)\rvert > 2.5)$	≥ 0	≥ 0	≥ 0	$= 1$
$D_{1(2)}$	–	$0.3 < D_{1(2)} < 0.6$	–	$0.2 < D_{1(2)} < 0.4$

FCNC tqg BDT input variables

Table 2 Input variables to the two NNs

Variable	Definition
Variables common to the D_1 and D_2 NNs	
$p_{\mathrm{T}}(b)$	Transverse momentum of the b-tagged jet
$m(\ell b)$	Invariant mass of the charged lepton (ℓ) and the b-tagged jet (b)
$m_{\mathrm{T}}(W)$	Transverse mass of the reconstructed W boson
$\Delta R(W, b)$	Distance in the η–ϕ plane between the reconstructed W boson and the b-tagged jet
$\lvert\Delta\phi(W, b)\rvert$	Azimuthal angle between the reconstructed W boson and the b-tagged jet
$m(\ell\nu b)$	Top-quark mass reconstructed from the charged lepton, neutrino, and b-tagged jet
Variables used only for the D_1 NN	
sgn $q(\ell)$	Sign of the charge of the primary lepton
$H_{\mathrm{T}}(\ell, b, E_{\mathrm{T}}^{\mathrm{miss}})$	Scalar sum of the transverse momenta of all reconstructed objects
$\eta(W)$	Pseudorapidity of the reconstructed W boson
$\lvert\Delta\phi(\ell, \vec{p}_{\mathrm{T}}^{\mathrm{miss}})\rvert$	Azimuthal angle between the charged lepton and $\vec{p}_{\mathrm{T}}^{\mathrm{miss}}$.
$\lvert\Delta\phi(W, \ell)\rvert$	Azimuthal angle between the reconstructed W boson and the charged lepton
$p_{\mathrm{T}}(\ell\nu b)$	Transverse momentum of the reconstructed top quark
Variables used only for the D_2 NN	
$\eta(b)$	Pseudorapidity of the b-tagged jet
$p_{\mathrm{T}}(W)$	Transverse momentum of the reconstructed W boson
$\Delta R(\ell\nu b, W)$	Distance in the η–ϕ plane between the reconstructed top quark and W boson

FCNC tqg NN discriminants

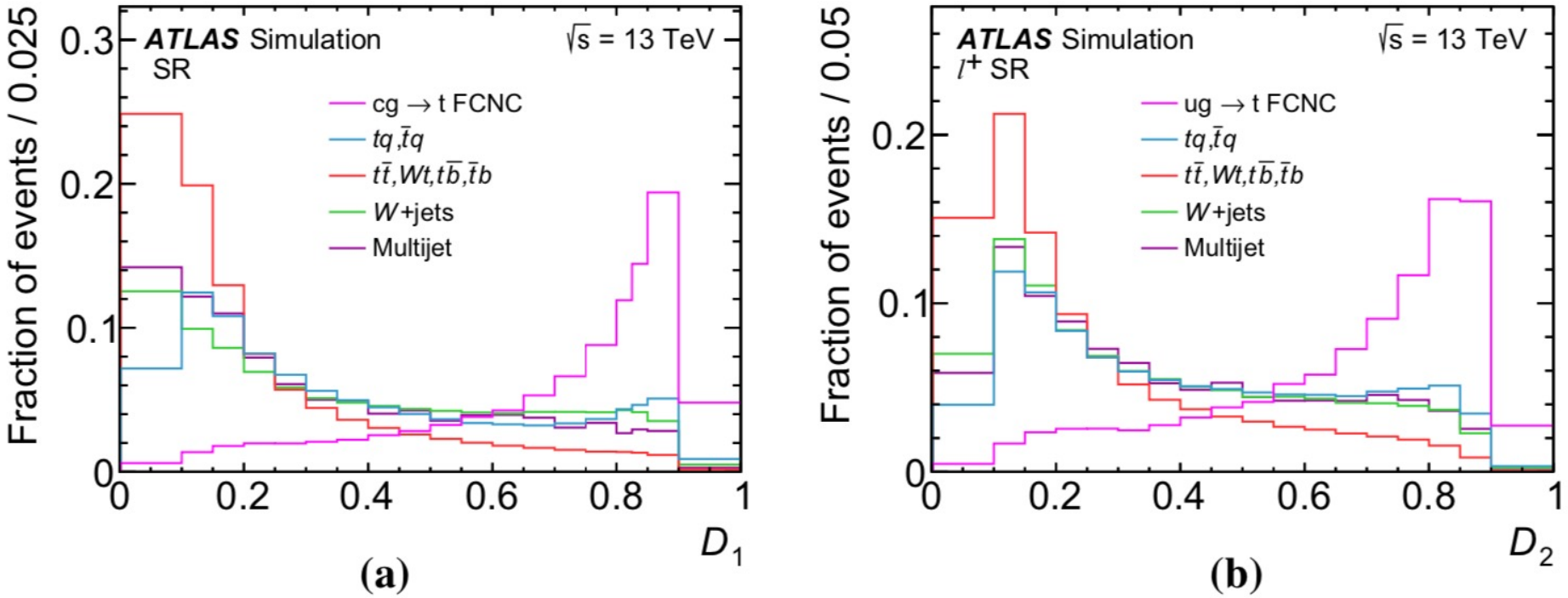

Fig. 4 Distributions of the D_1 and D_2 discriminants for signal and background processes. Each distribution is normalised to unit area. The discriminant D_1 was used for cgt analysis and the ℓ^- channel of the ugt analysis. The discriminant D_2 was used in the ℓ^+ channel of the ugt analysis. The histograms in (**a**) show the distributions obtained in the cgt analysis, that is, the discriminant was evaluated for all selected events independent of sgn $q(\ell)$. The distributions in the ℓ^+ channel of the ugt analysis are shown in (**b**)

FCNC tqg NN discriminants

Fig. 5 Distributions of the NN discriminants D_1 and D_2 observed in **a** the tqVR, **b** the $t\bar{t}$ VR and **c** the ℓ^+ W+jetsVR. The observed data are compared with the distribution of simulated background events normalised to the number of expected events, accounting for the normalisation factors obtained in the fits of the $E_{\mathrm{T}}^{\mathrm{miss}}$ and $m_{\mathrm{T}}(W)$ distributions for estimating the multijet background. The uncertainty band represents the uncertainty due to limited sample size and the rate uncertainties of the different processes (20% for W+jets production, 30% for the multijet background and 6% for the top-quark processes). The ratio of observed to predicted (Pred.) numbers of events in each bin is shown in the lower panel